(4)

AFGL-TR-88-0187

Kinetic, Thermochemical, and Phtodissociation Studies of Sulfur-Containing Atmospheric Ions

Timothy F. Thomas

University of Missouri
Department of Chemistry
5100 Rockhill Road
Kansas City, MO 64110

29 August 1988

Final Report
1 August 1984-30 September 1987

AIR FORCE GEOPHYSICS LABORATORY
AIR FORCE SYSTEMS COMMAND
UNITED STATES AIR FORCE
HANSCOM AIR FORCE BASE, MASSACHUSETTS 01731-5000

This technical report has been reviewed and is approved for publication.

JOHN F. PAULSON
Contract Manager

JOHN F. PAULSON
Acting Branch Chief

FOR THE COMMANDER

ROBERT A. SKRIVANEK, Director
Ionospheric Physics Division

This report has been reviewed by the ESD Public Affairs Office (PA) and is releasable to the National Technical Information Service (NTIS).

Qualified requestors may obtain additional copies from the Defense Technical Information Center. All others should apply to the National Technical Information Service.

If your address has changed, or if you wish to be removed from the mailing list, or if the addressee is no longer employed by your organization, please notify AFGL/DAA, Hanscom AFB, MA 01731. This will assist us in maintaining a current mailing list.

Do not return copies of this report unless contractual obligations or notices on a specific document requires that it be returned.

Unclassified

SECURITY CLASSIFICATION OF THIS PAGE

REPORT DOCUMENTATION PAGE

1a. REPORT SECURITY CLASSIFICATION Unclassified	1b. RESTRICTIVE MARKINGS
2a. SECURITY CLASSIFICATION AUTHORITY	3. DISTRIBUTION / AVAILABILITY OF REPORT Approved for public release; Distribution unlimited
2b. DECLASSIFICATION / DOWNGRADING SCHEDULE	
4. PERFORMING ORGANIZATION REPORT NUMBER(S)	5. MONITORING ORGANIZATION REPORT NUMBER(S) AFGL-TR-88-0187
6a. NAME OF PERFORMING ORGANIZATION Department of chemistry University of Missouri-KC 6b. OFFICE SYMBOL (If applicable)	7a. NAME OF MONITORING ORGANIZATION Air Force Geophysics Laboratory
6c. ADDRESS (City, State, and ZIP Code) 5100 Rockhill Road Kansas City, MO 64110	7b. ADDRESS (City, State, and ZIP Code) Hanscom AFB Massachusetts 01731-5000
8a. NAME OF FUNDING / SPONSORING ORGANIZATION 8b. OFFICE SYMBOL (If applicable)	9. PROCUREMENT INSTRUMENT IDENTIFICATION NUMBER F19628-84-K-0038
8c. ADDRESS (City, State, and ZIP Code)	10. SOURCE OF FUNDING NUMBERS PROGRAM ELEMENT NO. 61102F; PROJECT NO. 2303; TASK NO. G1; WORK UNIT ACCESSION NO. AG

11. TITLE (Include Security Classification) Kinetic, Thermochemical, and Photodissociation Studies of Sulfur-Containing Atmospheric Ions.

12. PERSONAL AUTHOR(S) Timothy F. Thomas

13a. TYPE OF REPORT	13b. TIME COVERED	14. DATE OF REPORT (Year, Month, Day)	15. PAGE COUNT
Final	FROM 84,Aug 1 TO 87,Sep 30	1988 August 29	44

16. SUPPLEMENTARY NOTATION

(+ or -)

17. COSATI CODES		
FIELD	GROUP	SUB-GROUP

18. SUBJECT TERMS (Continue on reverse if necessary and identify by block number)
Kinetics of Ion-Molecule Reactions, Ionization Potential, Appearance Potential, Mass Spectrometry, Thermochemistry of Ions, Sulfuric Acid, Sulfur Compounds, "Atmospheric chemistry" (AV)

19. ABSTRACT (Continue on reverse if necessary and identify by block number)
The rate constants of 25 reactions involving sulfur-containing ions or molecules at 298 K have been measured. Based on the results obtained a new condition for efficient charge transfer is proposed and reactions leading to formation of stratospheric ions with m/z=60, 78, and 98 are identified. The first complete mass spectra of sulfuric acid vapor have been obtained, its ionization potential has been found to be 12.40±.05 ev, and the appearance potentials for four of its fragment ions have been measured. From these data the $HOSO_2^+$-OH bond dissociation energy has been calculated to be 1.50±0.15 ev. A ion photofragment momentum spectrometer has been constructed and preliminary tests of its performance have been made. Keywords:)

20. DISTRIBUTION / AVAILABILITY OF ABSTRACT	21. ABSTRACT SECURITY CLASSIFICATION
☐ UNCLASSIFIED/UNLIMITED ☐ SAME AS RPT ☐ DTIC USERS	Unclassified
22a. NAME OF RESPONSIBLE INDIVIDUAL John Paulson	22b. TELEPHONE (Include Area Code) 617-377-3124
	22c. OFFICE SYMBOL APGL/LID

DD FORM 1473, 84 MAR 83 APR edition may be used until exhausted. All other editions are obsolete.

SECURITY CLASSIFICATION OF THIS PAGE

Unclassified

A. Summary of Work Accomplished

I. Analysis, Interpretation and Publication of Previously Acquired Data.

A significant fraction of the time spent by the principal investigator during the period of this contract was devoted to analysis of data acquired by him at AFGL during 1981-1983. This work resulted in two major publications, "The Photodissociation Spectrum of SO_2^+" and "Rate Constants for quenching the $\tilde{A}\ ^2A_2$ State of SO_2^+ by Atmospheric Gases," reprints of which are attached to this report. The first paper reports absolute cross sections for the photodissociation of SO_2^+ over the ranges 3000-3400 and 4400-5120Å and 6 spectroscopic constants for the $\tilde{A}$ state, 4 for the $\tilde{C}$ state, and 4 (tentative) for the $\tilde{D}$ state of the ion. It also resolved controversy over the assignment of the $\tilde{C}$ ($^2B_1$) and $\tilde{D}$ ($^2B_2$) states and identified the latter state as the source of the small yield of S^+ photoproduct observed for $\lambda_{irr} \leq 3108$Å.

The second paper analyzed the dependence of photodissociation cross sections for SO_2^+ upon ion source pressure and derived rate constants for quenching specific vibrational levels in the $\tilde{A}$ state of the ion. In three cases(with Q = SO_2 and N_2O) the quenching rate constants were greater than theoretically-predicted thermal capture rate constants, by factors ranging from 2.2 to 6.5. These anomalous results were explained in terms of several resonant or near-resonant charge transfer processes occurring in each case, and it was proposed that many more reactions having $k_{cE} >> k_{Th}$ can be discovered by studying state-to-state reactions between ions and molecules which have $\Delta E < RT$.

II. Measurement of Rate Constants for Ion-Molecule Reactions of Atmospheric Sulfur Compounds.

In order to assess the possible significance of ions of the general formula $H_xSO_y^+$ in the ion chemistry of the stratosphere and to test possible mechanisms for their formation, the rate constants of 25 reactions involving sulfur-containing molecules or ions were measured using the Selected Ion Flow Tube at AFGL during the summer of 1985.

The results obtained, organized according to reaction-type, are presented in Tables I-III along with literature values, where available ("k_{lit}"). Theoretical values ("k_{th}"), calculated according to the equations of Su and Chesnavich, are also shown, along with the enthalpy changes (ΔH) for the reactions. All measurements were made at 298 K and $N_{He}=1.3 - 1.8 \times 10^{16}$ atoms/cm^3.

The log of the ratio of the experimental rate constant to k_{th} is plotted versus- ΔH in Figure 1 for the change-transfer reactions listed in Table I. The data suggest the condition: $0 \leq - \Delta H \leq 1$ ev for efficient charge transfer, which is a special case of energy transfer from an electronically excited molecule. In Table III T is the calculated lifetime of the ion-molecule collision complex in the usual mechanism for a termolecular reaction.

In addition to the data reported in Table I-III upper limits of 10^{-11} cm^3 s^{-1} were found for the reactions:

1) $SO_3^+ + O_2 \rightarrow O_2^+ + SO_3$

$\rightarrow SO_4^+ + O$

$\rightarrow SO_3^+ \cdot O_2$

and,

2) $H_3O^+ \cdot H_2O + SO_2 \rightarrow H_3O^+ \cdot (H_2O)(SO_2)$

The following reaction was found to occur at an insignificant rate with respect to the competing charge transfer:

3) $SO_2^+ + O_2 \rightarrow SO_4^+$

The results obtained in this part of the project indicate that the following reactions may be important in forming the underlined ions in the stratosphere:

Table I. Rate Coefficients for Charge Transfer

	Reaction	Product Ratio(%)	$10^{10}xk_{exp}$ ($cm^3.s^{-1}$)	$10^{10}xk_{lit}$ ($cm^3.s^{-1}$)	$10^{10}xk_{th}$ ($cm^3.s^{-1}$)	ΔH (ev)
1)	$Ar^+ + SO_2 \rightarrow SO_2^+ + Ar$	87	3.4	4.8[1]	18.6	-3.47
	$S^+ + O_2 + Ar$	13				+0.56
2)	$SO_2^+ + NO \rightarrow NO^+ + SO_2$	92	1.0_7	---	7.2	-3.03
	$NO_2^+ + SO$	8				-0.12
3)	$SO_2^+ + NO_2 \rightarrow NO_2^+ + SO_2$	90	3.6_1	---	8.6	-2.67
	$NO^+ + SO_3$	10				-3.46
4)	$COS^+ + NO \rightarrow NO^+ + COS$	82	1.0_4	0.7[2]	7.3	-1.93
	$NS^+ + CO_2$	18				-2.03
5)	$COS^+ + NO_2 \rightarrow NO_2^+ + COS$	57	1.6_5	---	8.8	-1.56
	$NO^+ + CO + SO$	43				-0.94
6)	$S^+ + NO \rightarrow NO^+ + S$	100	4.1_2	3.7[2]	8.3	-1.09
7)	$SO^+ + NO \rightarrow NO^+ + SO$	100	8.2	---	7.6	-1.05
8)	$O_2^+ + COS \rightarrow COS^+ + O_2$	100	11.0	10.[3]	14.2	-0.89

Rate Coefficients for Charge Transfer (Continued)

	Reaction	Product Ratio(%)	$10^{10}xk_{exp}$ ($cm^3 \cdot s^{-1}$)	$10^{10}xk_{lit}$ ($cm^3 \cdot s^{-1}$)	$10^{10}xk_{th}$ ($cm^3 \cdot s^{-1}$)	ΔH (ev)
9)	$SO^+ + NO_2 \rightarrow NO_2^+ + SO$	72	7.2	---	9.2	-0.69
	$NO^+ + SO_2$	28				-3.59
10)	$H_2O^+ + SO_2 \rightarrow SO_2^+ + H_2O$	100	28.	---	24.7	-0.33
11)	$SO_2^+ + O_2 \rightarrow O_2^+ + SO_2$	100	2.6	2.8[4]	6.4	-0.21
12)	$SO_2^+ + H_2O \rightarrow H_2O^+ + SO_2$	100	12.0	---	23.9	+0.33

1) N.G. Adams and D. Smith, Int. J. Mass Spectrom. Ion Phys. 21, 349 (1979).

2) D. Smith, N.G. Adams, and W. Lindinger, J. Chem. Phys. 75, 3365 (1981).

3) D. Smith, N.G. Adams, T.M. Miller, J. Chem. Phys. 69, 308 (1978).

4) F.C. Fehsenfeld and E.E. Ferguson, J. Geophys. Res. 78, 1699 (1973).

Table II. Rate Coefficients for Atom Exchange

	Reaction	Product Ratio(%)	$10^{10}xk_{exp}$ ($cm^3 \cdot s^{-1}$)	$10^{10}xk_{lit}$ ($cm^3 \cdot s^{-1}$)	$10^{10}xk_{th}$ ($cm^3 \cdot s^{-1}$)	ΔH (ev)
1)	$SO^+ + NO_2 \rightarrow NO^+ + SO_2$	28	2.0_2	---	9.2	-3.59
2)	$SO_2^+ + NO_2 \rightarrow NO^+ + SO_3$	10	0.36	---	8.6	-3.46
3)	$COS^+ + NO \rightarrow NS^+ + CO_2$	18	0.19	---	7.3	-2.03
4)	$SO^+ + N_2O \rightarrow SO_2^+ + N_2$	100	0.61	---	8.8	-2.01
5)	$COS^+ + NO_2 \rightarrow NO^+ + CO + SO$	43	0.71	---	8.8	-0.94
6)	$SO_2^+ + NO \rightarrow NO_2^+ + SO$	8	0.09	---	7.2	-0.12

Table III. Rate Coefficient for Clustering Reactions. T=298°K

	Reaction	Product Ratio(%)	$10^{-16} x N_{He}$ (cm^{-3})	$10^{27} x k_{ter}$ ($cm^6 \cdot s^{-1}$)	$10^{27} x k_{lit}$ ($cm^6 \cdot s^{-1}$)	$10^{10} x \cdot$ (s)
1)	$SO_3^+ + H_2O \rightarrow H_2SO_4^+$	100	1.14-1.70	4.5	---	36
2)	$SO_2^+ + SO_2 \rightarrow S_2O_4^+$	100	1.30	2.1	---	24
3)	$SO^+ + SO_2 \rightarrow S_2O_3^+$	100	1.30	1.0	---	10.5
4)	$COS^+ + H_2O \rightarrow H_2CO_2S^+$	100	1.29-1.85	1.2	<0.007[2]	9.0
5)	$H_3O^+ + SO_2 \rightarrow H_3SO_3^+$	100	1.31-1.32	1.0	---	7.7
6)	$SO^+ + H_2O \rightarrow H_2SO_2^+$	100	1.31-1.91	0.76	---	5.6
7)	$O_2^+ + SO_2 \rightarrow SO_4^+$	91	1.63-1.74	0.41	0.6[3]	3.8

1) $k_{ter} = k_{exp}/N_{He}$

2) D. Smith, N.G. Adams, and W. Lindinger. J. Chem. Phys. 75, 3365 (1981).

3) N.G. Adams, D.K. Bohme, D.B. Dunkin, F.C. Fehsenfeld, and E.E. Ferguson, J. Chem. Phys., 52, 3133 (1970). At T = 200 K. P = 0.4-2.0 Torr in flowing afterglow system.

RATE COEFFICIENTS FOR CHARGE TRANSFER

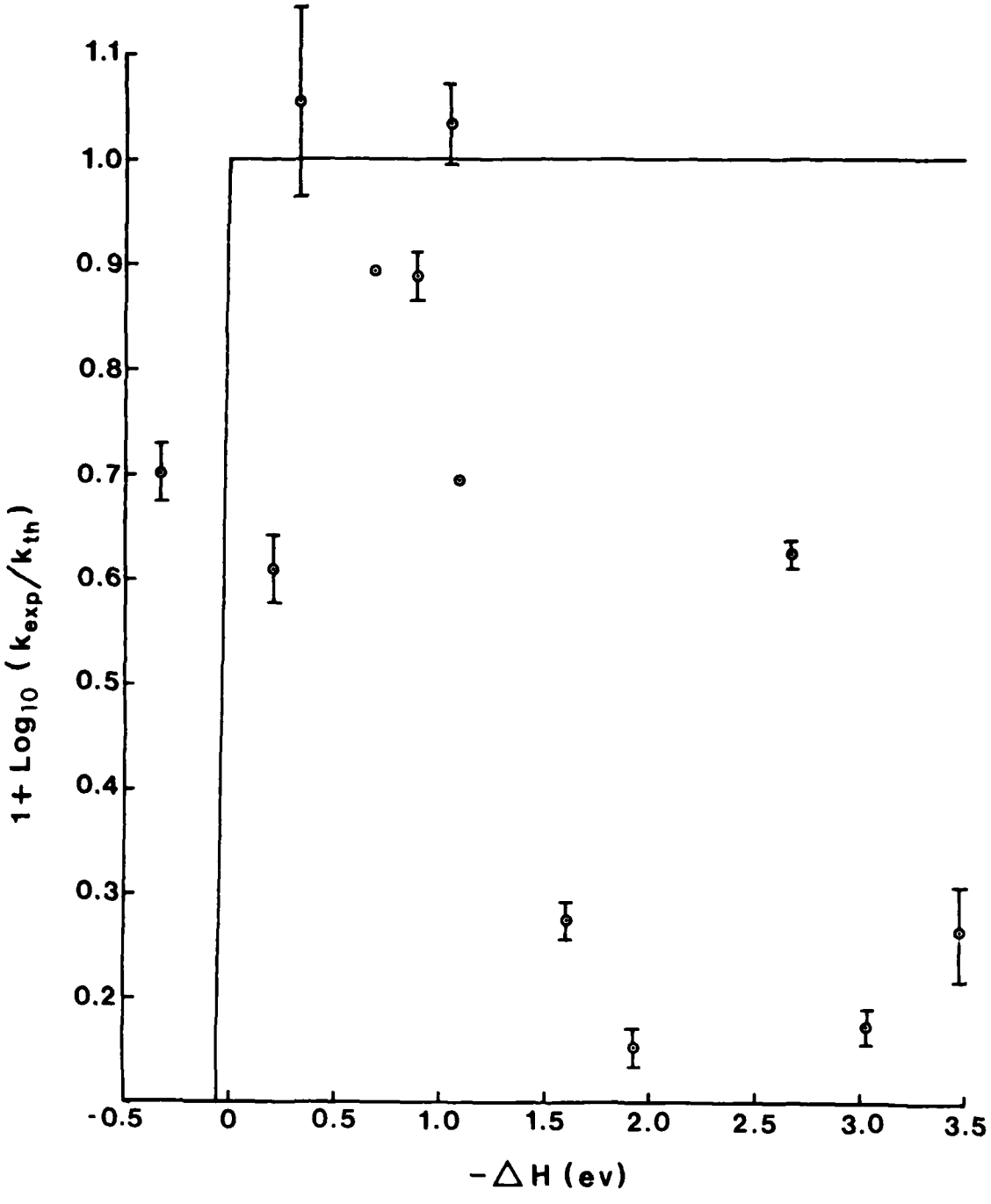

Figure 1

4) $SO_3^+ + H_2O \xrightarrow{k=3\times10^{-27}cm^6\ s^{-1}} \underline{H_2SO_4^+}\ (\frac{m}{z} = 98)$

5) $O_2^+ + OCS \xrightarrow{k=1.1\times10^{-9}cm^3\ s^{-1}} \underline{OCS^+}\ (\frac{m}{z} = 60) + O_2$

6) $OCS^+ + H_2O \xrightarrow{k=1.2\times10^{-27}cm^6\ s^{-1}} OCS^+ \cdot H_2O (\frac{m}{z} = 78)$

Further measurements of the rate constants for these reactions at the lower temperature prevailing in the stratosphere should be carried out.

III. Thermochemistry of $H_xSO_y^+$ Ions.

The major effort during the contract period was devoted to obtaining the mass spectrum, ionization potential, and appearance potentials for fragment ions of sulfuric acid vapor. After much trial and failure an inlet system was constructed which delivered H_2SO_4 into the ion source of our Nuclide mass spectrometer with a minimum of surface reactions (as evidenced by a decline of the SO_2^+ peak and the appearance of an SO_3^+ peak in the mass spectrum of the vapor). By gold-plating each part of the RPD ion source exposed to the incoming H_2SO_4 vapor it also proved possible to observe the molecular ion of H_2SO_4, for the first time.

The mass spectrum of the azeotrope of $H_2SO_4 + H_2O$ ($\sim$98.3% H_2SO_4 by weight), obtained after 100 hours of pumping on a 5 ml liquid sample of H_2SO_4 + 6% SO_3, is shown in Figures 2 and 3. The same sample and ion source conditions were used for each

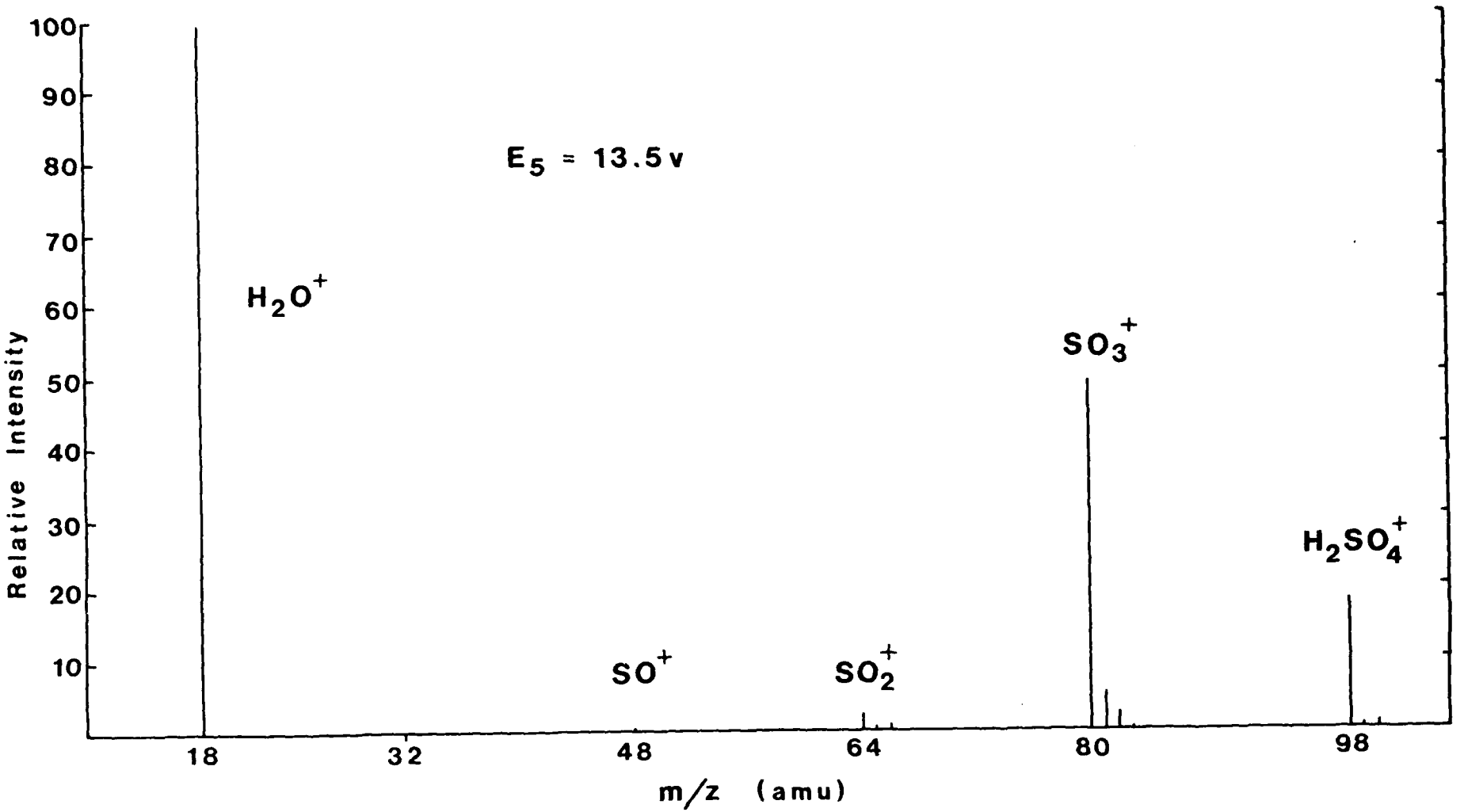
MASS SPECTRUM OF H_2SO_4
(Vapor from Azeotrope at 351°K)
$T_{ion\ source}$ = 381°K
E_5 = 13.5v
Relative Intensity
100
90
80
70
60
50
40
30
20
10
H_2O^+
SO^+
SO_2^+
SO_3^+
$H_2SO_4^+$
18
32
48
64
80
98
m/z (amu)

Figure 2

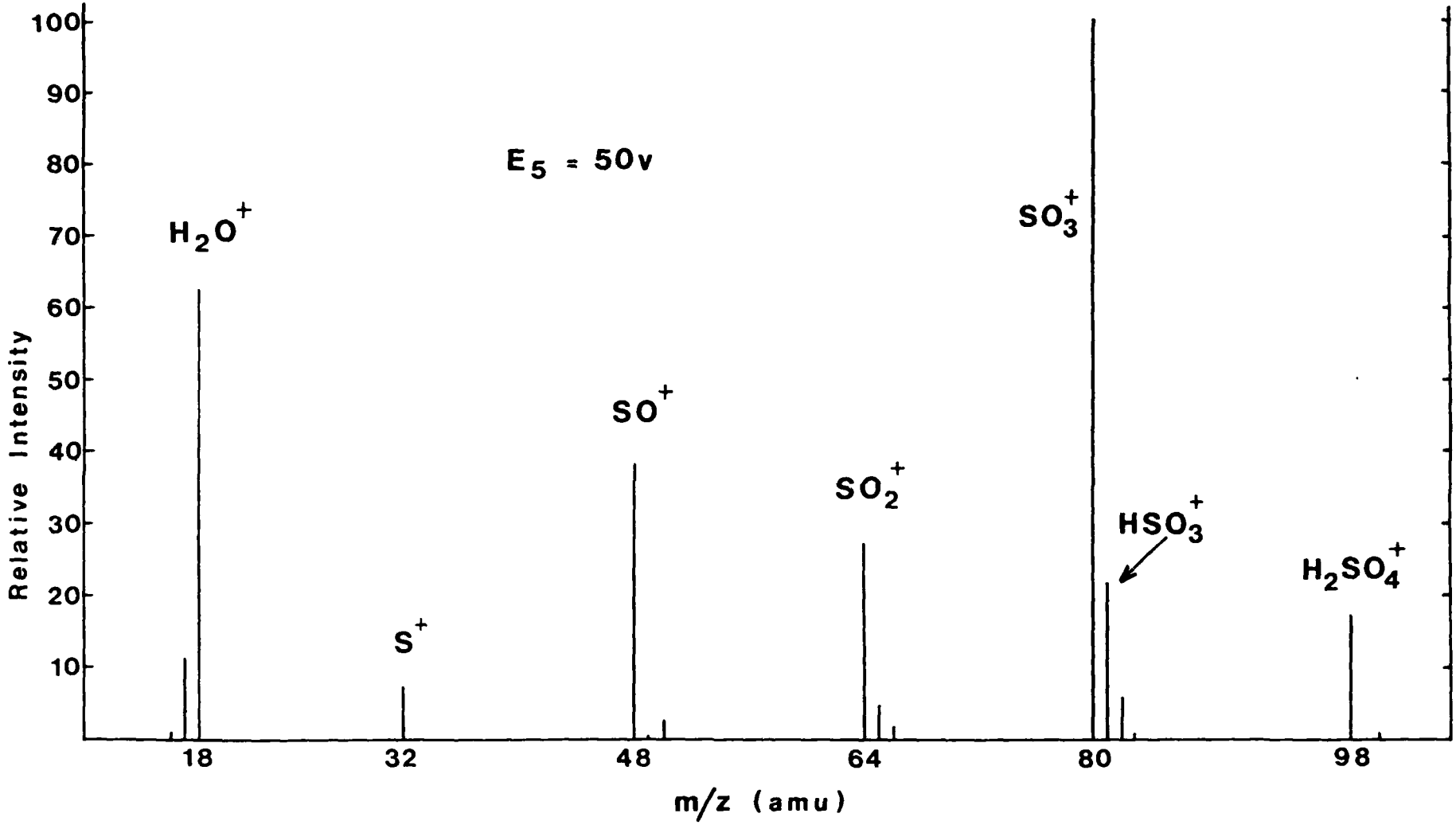
100
90
80
70
60
50
40
30
20
10
Relative Intensity
E_5 = 50v
H_2O^+
S^+
SO^+
SO_2^+
SO_3^+
HSO_3^+
$H_2SO_4^+$
18
32
48
64
80
98
m/z (amu)

Figure 3

spectrum. The quanitity "E_5" is the energy of the electrons entering the ionization region. The relative intensities of the mass spectral peaks were found to be strongly dependent on the temperature of the ion source. As shown by Figure 4 this effect probably results from the shifting of the following equilibrium as the H_2SO_4 vapor is heated from 349 K in the sample reservoir to 365-425 K in the ion source:

7) $H_2SO_4(g) \rightleftharpoons SO_3(g) + H_2O(g)$.

The upper line in the Figure assumes that the $H_2SO_4^+$, SO_3^+, and H_2O^+ intensities are directly proportional to only the concentrations of the corresponding neutrals in the ion source. The lower line shows an attempt to correct for the fact that some H_2O^+ is formed from H_2SO_4 at an electron impact energy of 13.5ev. The enthalpy of reaction for (7) calculated from the slopes of the lines in Figure 4 is 3.5-7.0 Kcals/mol greater than the ΔH_{dissoc}=24.6 Kcal/mol calculated from the JANAF Thermochemical Tables (3rd Edition). This small discrepancy may result from failure of the vapor to reach equilibrium during its flow from the sample vessel through the heated inlet and vacuum housing into the ion source.

Ionization and appearance potential measurements were made using a Fox-type retarding potential difference (RPD) ion source, operating with a modulation width of 0.1 v on the second and third plates of the electron gun. Figure 5 shows typical ionization efficiency curves obtained for three of the ions formed from H_2SO_4 vapor in addition to one from Xe, one of the two reference gases used to calibrate the scale for the electron energy. Figure 6 shows the result of scaling three of the curves to have the same slope over the last volt of each scan and Figure 7 shows the method of extrapolating the separation of pairs of curves (along the E5 scale) to the onset of ion formation. Table IV gives the ionization and appearance potentials which were obtained by this method, along with estimated uncertainties and literature values. In the cases of H_2O^+, SO_3^+, and SO_2^+ it was necessary to subtract a contribution from direct ionization of the small amounts of H_2O, SO_3, and SO_2 present in the sample stream from the total ionization

EFFECT OF ION SOURCE TEMPERATURE ON MASS SPECTRUM at $E_5 = 13.5v$

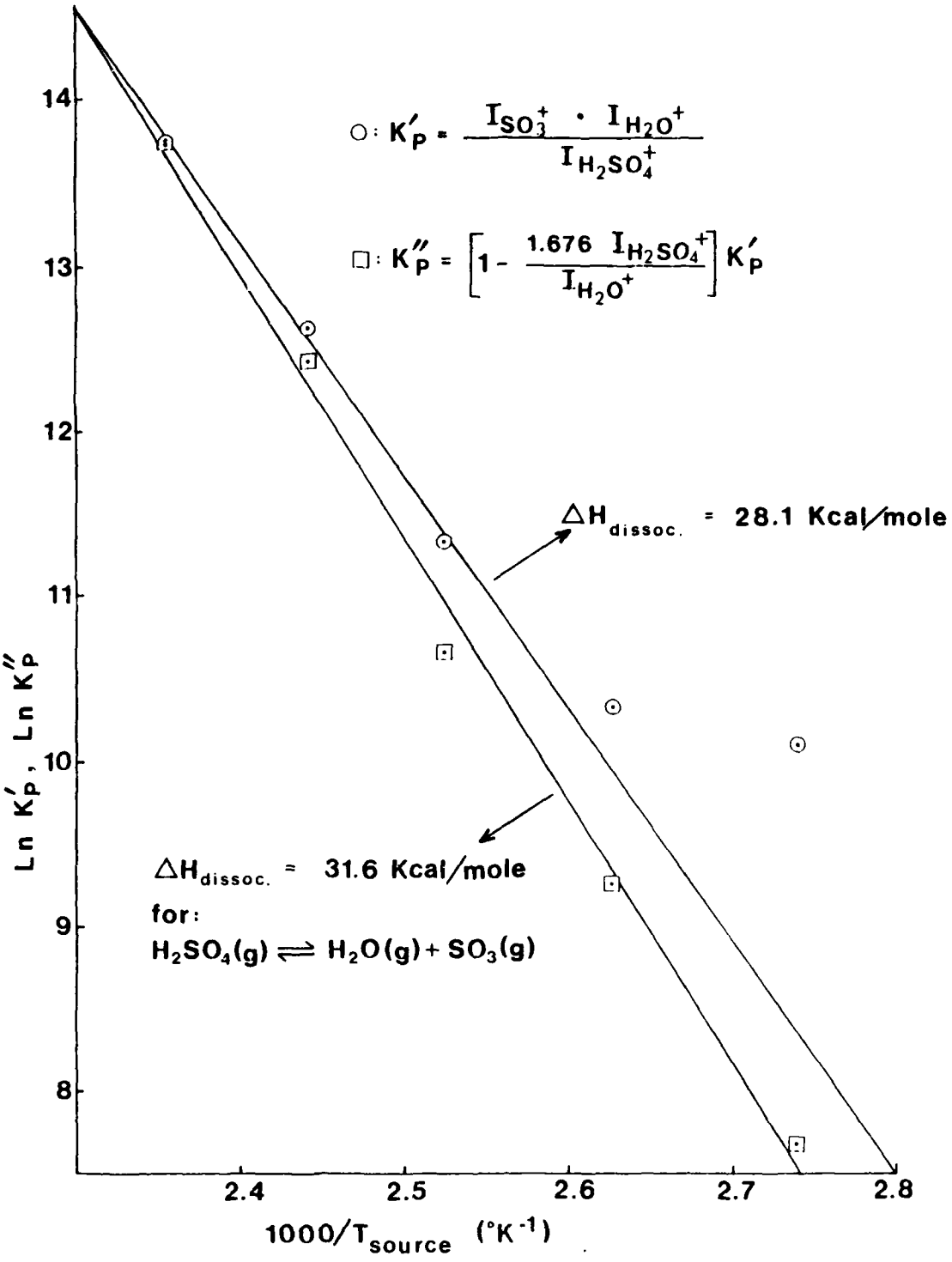

Figure 4

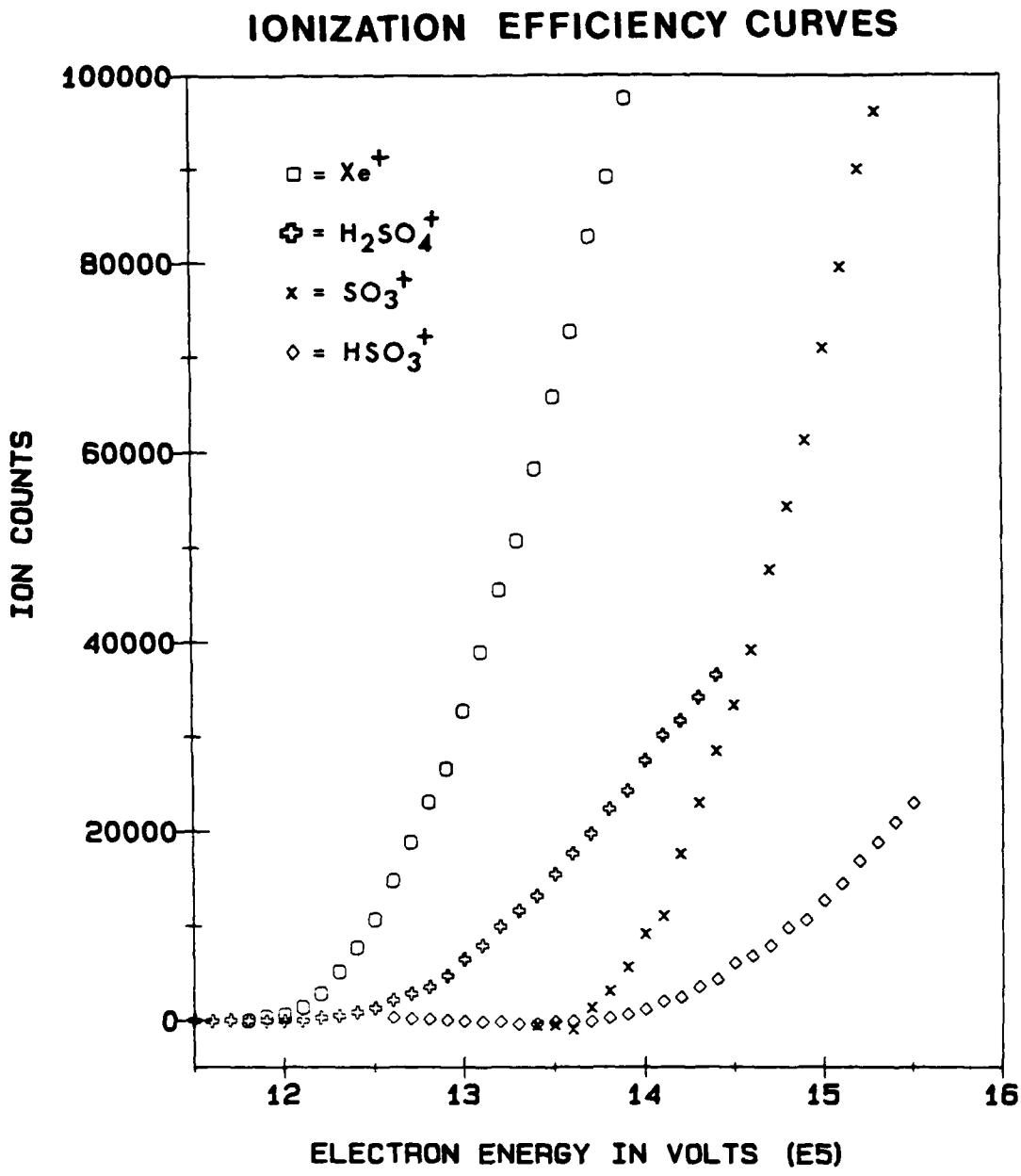
IONIZATION EFFICIENCY CURVES
100000
80000
60000
40000
20000
0
ION COUNTS
□ = Xe+
✣ = H2SO4+
x = SO3+
◇ = HSO3+
12
13
14
15
16
ELECTRON ENERGY IN VOLTS (E5)

Figure 5

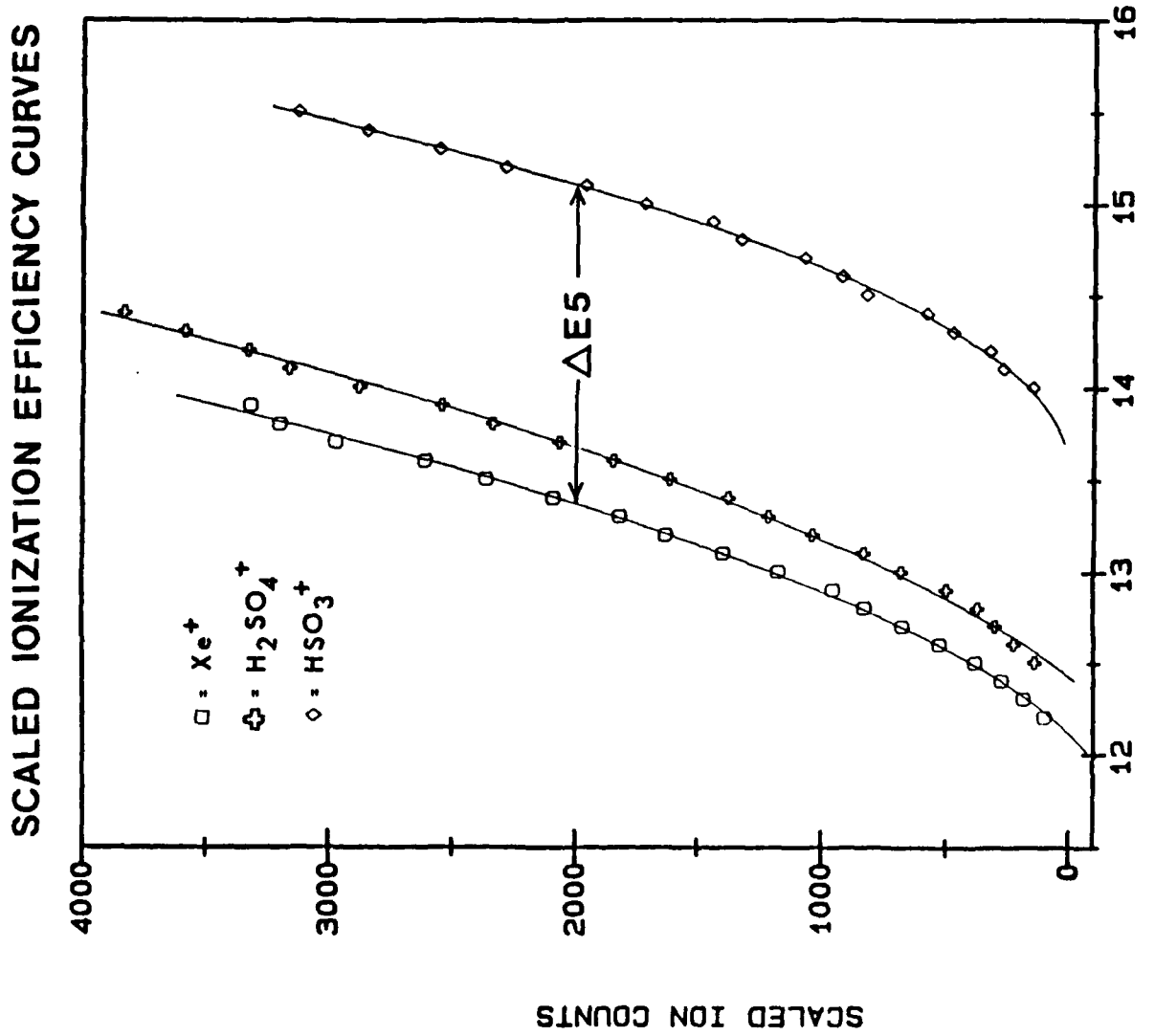
SCALED IONIZATION EFFICIENCY CURVES
□ = Xe^+
◇ = $H_2SO_4^+$
◇ = HSO_3^+
ΔE5
SCALED ION COUNTS
0
1000
2000
3000
4000
ELECTRON ENERGY IN VOLTS (E5)
12
13
14
15
16

Figure 6

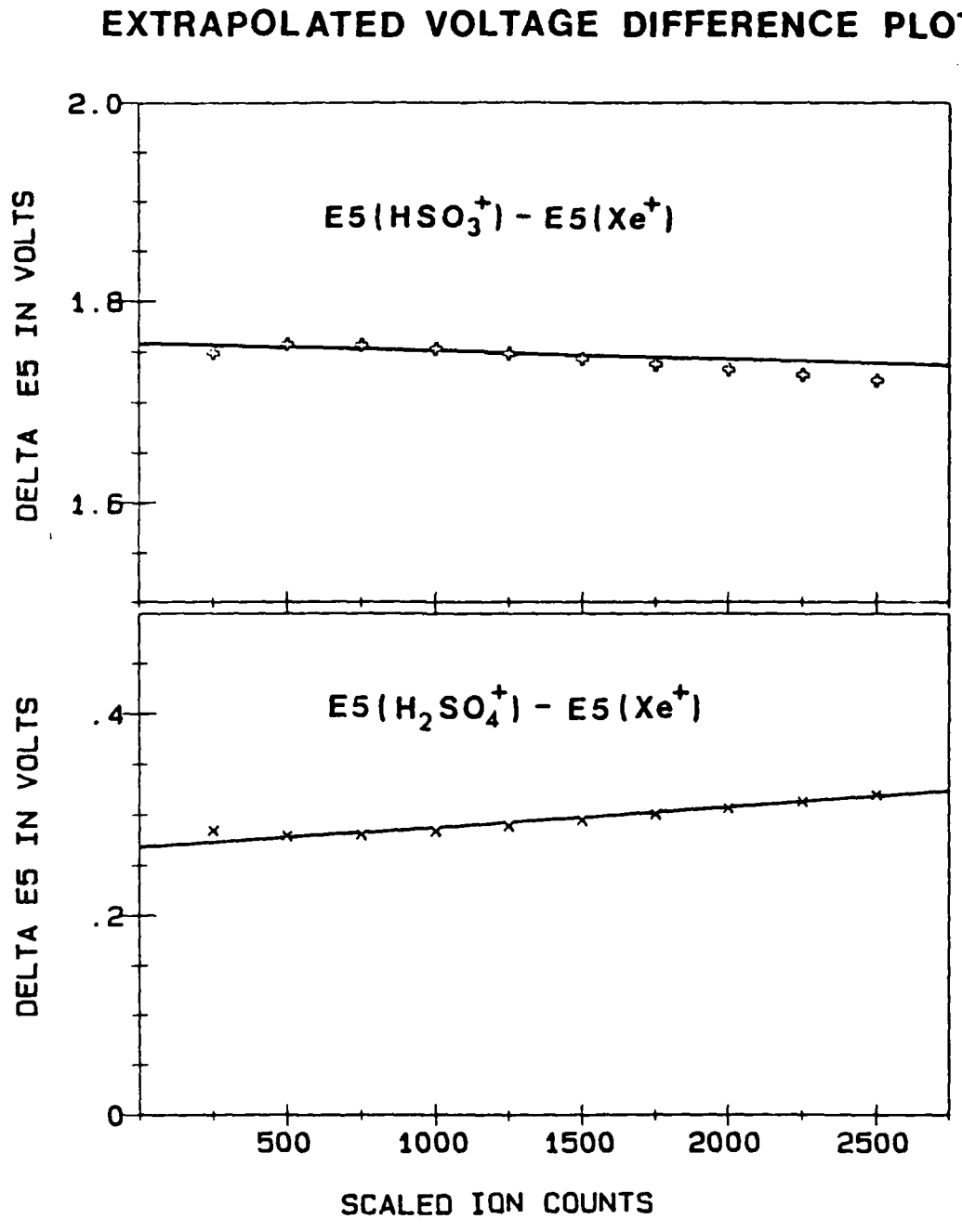
EXTRAPOLATED VOLTAGE DIFFERENCE PLOT
2.0
1.8
1.6
DELTA E5 IN VOLTS
E5(HSO3+) - E5(Xe+)
.4
.2
0
DELTA E5 IN VOLTS
E5(H2SO4+) - E5(Xe+)
500
1000
1500
2000
2500
SCALED ION COUNTS

Figure 7

Table IV. **Appearance energies for fragment ions from the components of sulfuric acid vapor.** T_{source} = 381 K.

No.	Reaction	A.E.(ev)	Lit. Value
1)	$H_2SO_4 \rightarrow H_2SO_4^+ + e^-$	$12.4_0 \pm p.05$	---
2)	$SO_2 \rightarrow SO_2^+ + e^-$	$12.5 \pm .1$	12.31(a),12.4(b)
3)	$H_2O \rightarrow H_2O^+ + e^-$	$12.6_5 \pm .05$	12.61(c)
4)	$SO_3 \rightarrow SO_3^+ + e^-$	$13.1_5 \pm .05$	12.80(c),13.2(b)
5)	$H_2SO_4 \rightarrow H_2O^+ + SO_3^+ e^-$	$13.2 \pm .2$	---
6)	$H_2SO_4 \rightarrow SO_3^+ + H_2O + e^-$	$13.8 \pm .2$	
7)	$H_2SO_4 \rightarrow HSO_3^+ + OH + e^-$	$13.9 \pm .1$	---
8)	$SO_3 \rightarrow SO^+ + O_2 + e^-$	$15.1 \pm .1$	14.8(b)
9)	$H_2SO_4 \rightarrow SO_2^+ + H_2O_2 + e^-$	$15.9_7 \pm .15$	---
10)	$SO_3 \rightarrow SO_2^+ + O + e^-$	$18.3_5 \pm .1$	18.3(b)

a) T.F. Thomas, F. Dale, and J.F. Paulson, J. Chem. Phys. 88, 5553 (1988).

b) O.I. Smith and J.S. Stevenson, J. Chem. Phys. 74, 6777 (1981).

c) S.G. Lias, et al., Gas Phase Ion and Neutral Thermochemistry, J. Phys. Chem. Ref. Data, 17, Suppl. No. 1 (1988).

efficiency courves obtained. Thus the indicated uncertainties are larger in these cases.

From the data in Table IV it is possible to calculate the enthalpy of formation for several species of interest. Table V presents this quantity for three sulfur-containing species derived from the data in Table IV. (Although the data are presented for "298 K," the appearance potential data were not adjusted from 381 K to 298 K in doing the calculations.) One other quantity of interest which may be calculated from the data in Table IV is the dissociation energy for the S-OH bond in $H_2SO_4^+$. The result is $DH^o(HO_3S^+\text{-}OH) = 1.5 \pm 0.15$ ev. For comparison, $DH^o(O_2S^+\text{-}O) = 5.2 \pm 0.15$ ev, can also be derived from Table IV.

IV. Photodissociation Spectroscopy of OCS^+

Construction of an ion photofragment momentum spectrometer was completed largely as proposed. Several modifications in the original plans were made as necessary including the acquisition of faster ion-counting electronics (EG&G Ortec 9301 Pre-Amplifier & 9302 Amplifier/Discriminator), acquisition of a multi-channel analyzer (Canberra 35+) with a 200 MHz multi-channel scalar (Canberra 7880), and installation of a new grating and calibration lamps for use with the government-supplied vacuum monochromator (for calibration of laser wavelengths). A Colutron Wien velocity filter was purchased as proposed but is not yet installed in the system.

Because of the unexpectedly long time required to complete the work on sulfuric acid described in the previous section, only preliminary tests were made of the newly assembled apparatus. Using a primary ion beam of $\sim 10^{-11}$ A of N_2O^+ (measured after passage through the 12" radius magnetic analyzer) a peak was found in the photodissociation spectrum at $\lambda_{irr}=3381.8$ Å in reasonable agreement with the $\lambda_{max}=3381.0 \pm 0.5$ Å previously obtained at AFGL. The measured photodissociation cross section was $0.8 \pm 0.6 \times 10^{-18}$ cm^2, compared with the previously published value of $4.0 \times 10^{-18} cm^2$, indicating that careful measurements of transmission ratios must be made

Table V. Enthalpies of Formation at 298 K (in Kcal/mole)

Specie	Source of Data	ΔH_f°	Lit. Value
H_2SO_4 (g)	AP(H_2O^+)	-166±5	-176[a]
H_2SO_4 (g)	AP(SO_3^+)	-176±5	-176[a]
$H_2SO_4^+$ (g)	IP of H_2SO_4	110±1	≤103[b]
HSO_3^+ (g)	AP(HSO_3^+)	135±2	133±2[c]

a) JANAF Thermochemical Tables, 3rd Edition (1985).

b) Based on the report by A. Viggiano, et al., J. Geophys Res. 85, 451 (1980), that charge transfer from O_2^+ to H_2SO_4 occurs at every collision.

c) S.G. Lias, et al., Gas Phase Ion and Neutral Thermochemistry, J. Phys. Chem. Ref. Data 17, Suppl. No. 1 (1988).

and ion/laser beam overlap must be evaluated. The pulse energy used above was only $3x10^{-5}$J and the light path length through the ion beam was 0.16 cm.

Since the end of the contract period, a pair of prisms has been inserted within the photodissociation region which has increased the light path through the ion beam to 0.63 cm, and a "Fred Dale" ion source has been installed which routinely delivers ion beam currents of $4x10^{-10}$ A after the magnetic analyzer. With these improvements a photodissociation cross section of 2×10^{-20} cm^2 can now be measured with a statistical error of 30% for laser pulse energies of $1x10^{-3}$ Joule, a total of 3000 pulses, and a detector slit width of 1.3 mm. Work on this project is continuing, supported by a portion of the indirect costs which were charged to this contract, returned to the principal investigator under UMKC's research incentive program.

B. Presentations and Publications

1. T.F. Thomas, A,A. Viggiano, F. Dale, and J.F. Paulson, "Rate Constants for Ion-Molecule Reactions of Atmospheric Sulfur Compounds," paper No. 504, presented to the 21st Midwest Regional Meeting of the American Chemical Society, Nov. 6, 1986.

2. K.B. Snow and T.F. Thomas, "Appearance Potential Measurements on Sulfuric Acid Vapor," paper No. 853, presented to the 21st Midwest Regional Meeting of the American Chemical Society, Nov. 6, 1988.

3. K.B. Snow and T. F. Thomas, "Appearance Potential Measurements on Sulfuric Acid Vapor," paper No. MPA15, presented to the 36th ASMS Conference on Mass Spectrometry, June 6, 1988.

4. T.F. Thomas, A.A. Viggiano, F. Dale and J.F. Paulson, "Rate Constants for Ion-Molecule Reactions of Atmospheric Sulfuric Compounds," paper No. TPB 36, presented to the 36th ASMS Conference on Mass Spectrometry, June 7, 1988.

5. T.F. Thomas, F. Dale, and J.F. Paulson, "The Photodissociation Spectrum of SO_2^+," J. Chem. Phys., 84, 1216-1227 (1986).

6. T.F. Thomas, F. Dale, and J.F. Paulson, "Rate Constants for Quenching the $\tilde{A}\ ^2A_2$ State of SO_2^+ by Atmospheric Gases," J. Chem. Phys., 88, 5553-5560 (1988).

7. K.B. Snow and T.F. Thomas, "The Mass Spectrum, Ionization Potential, and Appearance Potentials for Fragment Ions of Sulfuric Acid Vapor," in manuscript (to be submitted to J. Phys. Chem.).

8. T.F. Thomas, A.A. Viggiano, F. Dale, and J.F. Paulson, "Rate Constants for Ion-Molecule Reactions of Atmospheric Sulfur Compounds," in preparation.

The photodissociation spectrum of SO_2^+

Timothy F. Thomas[a)]
Department of Chemistry, University of Missouri-Kansas City, Kansas City, Missouri 64110

Fred Dale and John F. Paulson
Air Force Geophysics Laboratory/LID, Hanscom AFB, Massachusetts 01731

(Received 20 June 1985; accepted 22 October 1985)

The photodissociation spectrum of SO_2^+ corresponding to the process $SO_2^+ + h\nu \rightarrow SO^+ + O$ has been measured on a triple quadrupole system for the wavelength ranges: 3000–3400 and 4400–5120 Å. The spectrum in the visible has been assigned to the $\tilde{C}\,^2B_1 \leftarrow \tilde{A}\,^2A_2$ transition and vibrational structure analyzed to yield $\lambda_{00} = 4187$ Å, the harmonic vibrational frequencies $\tilde{\nu}_1'' = 953\ cm^{-1}$, $\tilde{\nu}_2'' = 499\ cm^{-1}$, $\tilde{\nu}_1' = 767\ cm^{-1}$, and $\tilde{\nu}_2' = 410\ cm^{-1}$, and the anharmonicity constants $X_{11}'' = -6.3\ cm^{-1}$, $X_{12}'' = -6.1\ cm^{-1}$, $X_{22}'' = -4.2\ cm^{-1}$, $X_{12}' = -6.3\ cm^{-1}$, and $X_{22}' = -7.4\ cm^{-1}$. Apparent photodissociation cross sections ranged from $\sim 1\times10^{-20}$–$1.6\times10^{-19}\ cm^2$ in the visible spectrum. In the UV spectrum the highly congested vibrational structure could not be resolved sufficiently for analysis; photodissociation cross sections ranged from ~ 2–$4\times10^{-19}\ cm^2$ with broad bands roughly corresponding to expected progression in ν_1' and ν_2' within the $\tilde{C}\,^2B_1 \leftarrow \tilde{X}\,^2A_1$ electronic transition. The process $SO_2^+ + h\nu \rightarrow S^+ + O_2$ showed an onset near 3108 Å and the corresponding photodissociation spectrum showed sufficient vibrational structure to yield $\tilde{\nu}_2'' \sim 454\ cm^{-1}$, $\tilde{\nu}_1' \sim 955\ cm^{-1}$, and $\tilde{\nu}_2' \sim 411\ cm^{-1}$. This new process, which had $\sigma < 3\times10^{-20}\ cm^2$, was proposed to result from the $\tilde{D}\,^2B_2 \leftarrow \tilde{X}\,^2A_1$ transition. Several new photodissociation cross section measurements on N_2O^+ have also been made in the vicinities of 3381 and 4880 Å, taking advantage of the high sensitivity ($\rightarrow 10^{-21}\ cm^2$) of the triple quadrupole system.

I. INTRODUCTION

Sulfur dioxide has been detected in the stratosphere at relative concentrations of ~ 50 ppb,[1] roughly 1/10 the concentration of NO,[2] whose important role in the ion chemistry occurring at higher altitudes (the D region of the ionosphere) is well established.[3] Although its concentration varies strongly with such unpredictable events as volcanic eruptions,[4] SO_2 must be a major source of the sulfuric acid which constitutes the major component of the aerosol layer ("Junge layer") present in the lower stratosphere[5,6] and which extends beyond 35 km in molecular form (or as HSO_3).[7,8] Since efficient paths exist for forming the positive ion of SO_2 in the upper stratosphere, we hypothesized that photochemical and bimolecular reaction of SO_2^+ may ultimately lead to more complex and thus more stable sulfur-containing positive ions.[9] This would parallel the recently discovered role of H_2SO_4 in forming negative ion clusters between 15 and 40 km.[12–14]

A key step in forming sulfur-containing ions of potential importance in the positive ion chemistry of the stratosphere seemed likely to be the photodissociation of SO_2^+. As shown in Fig. 1, available photoelectron data on SO_2 led to the prediction of several allowed electronic transitions in SO_2^+ at wavelengths which can penetrate the ozone layer. The $\tilde{C}$ and $\tilde{D}$ states of SO_2^+ had previously been reported to be strongly predissociated with SO^+ as the only detectable ionic fragment.[16] And, although the relevant rate constants were not available, a sequence of exothermic reactions with O_2 and H_2O could be written to convert SO^+ into ions of the form $H_xSO_y^+$. It therefore seemed worthwhile to obtain the photodissociation spectrum of SO_2^+ above 2900 Å.[17] In addition, the recent report[18] that S^+ formation competes with SO^+ formation in a very narrow range of energy levels within the $\tilde{C}$ state of SO_2^+ offered the possibility of studying mode-specific effects on the photodissociation pathway.

II. EXPERIMENTAL METHOD

The photodissociation apparatus previously used in this laboratory[19,20] (tandem magnetic and quadrupole mass analyzers, with transverse irradiation of the ion beam) was converted into a triple quadrupole system with coaxial irradiation, following the example of Morrison and McGilvery.[21] As shown in Fig. 2 the output beam from a flashlamp-pumped tunable dye laser (Chromatix CMX-4) entered the vacuum system through a quartz window at the Brewster's angle, passed along the center line of the analyzer quadrupole, the reactor quadrupole (where the ion beam is confined by an rf field only), the source quadrupole (which selects the reactant ions), and out through a simple electron impact ion source. The ion source box had a 3.2 mm ion exit aperture, an external filament, no electron trap, and the repeller was replaced by a 6.4 mm o.d. stainless steel tube leading to an optical port. The laser beam exited this port through a Brewster's angle quartz window and entered the energy meter as shown in the diagram. A small fraction of this beam was reflected by the quartz entrance window of the energy meter to a photodiode which generated start pulses for the time-of-flight logic, as previously described.[19]

Since the source quadrupole rejected substantially all photoproduct ions formed in it and the analyzer quadrupole was tuned to reject any reactant ions, only photoproduct

[a)] AFOSR-URRP Visiting Professor at AFGL, 1981-3.

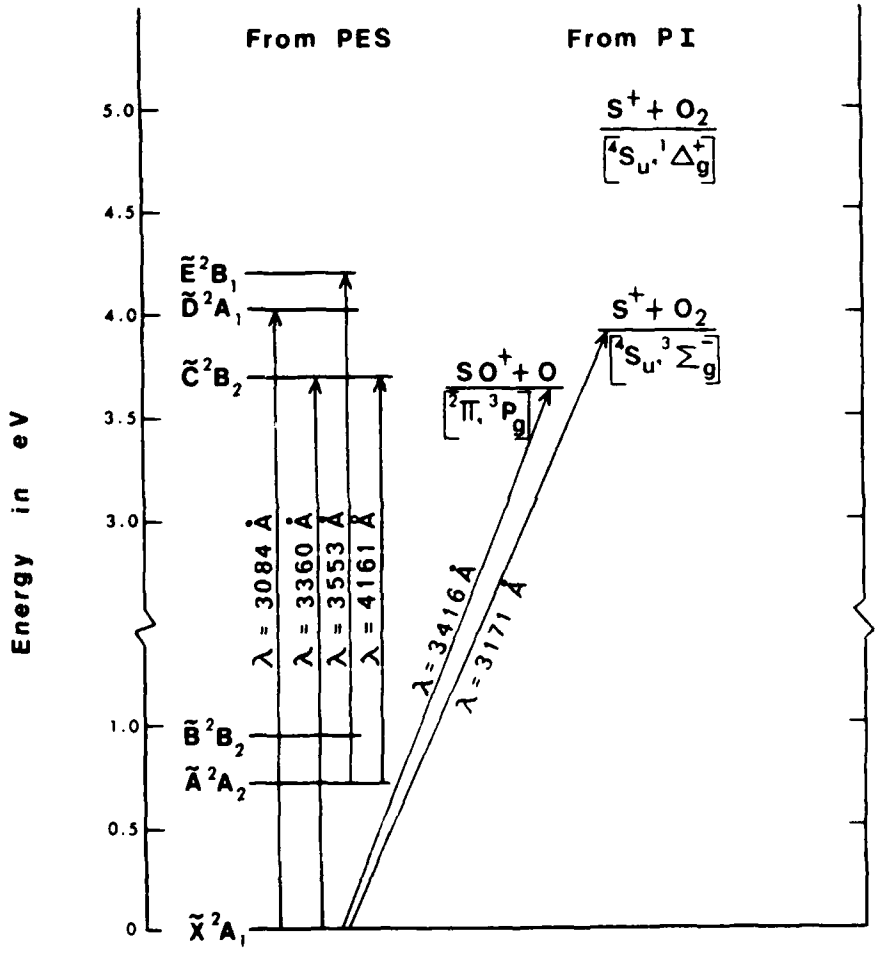

FIG. 1. Energy levels of SO_2^+ and its fragments. Threshold transition wavelengths were calculated from the data compiled in Ref. 15, and excited state symmetries were taken from the same source. For revised identification of the $\tilde{C}$, $\tilde{D}$, and $\tilde{E}$ states of SO_2^+ see Sec. III D.

ions formed in the 15.2 cm long reactor quadrupole were detectable. To discriminate further against photoproduct ions formed in the source quadrupole, the rods of the reactor quadrupole were normally biased to reject ions having kinetic energies less than or equal to 75% of the desired reactant ions. Typical ion energies were 16.0, 3.9, and 20.0 eV in the source, reactor, and analyzer quadrupole regions, respectively. The effect of the voltage and frequency of the rf signal applied to the reactor quadrupole was studied briefly (see Fig. 3). The value 400 VAC at 2.1 MHz was selected for use

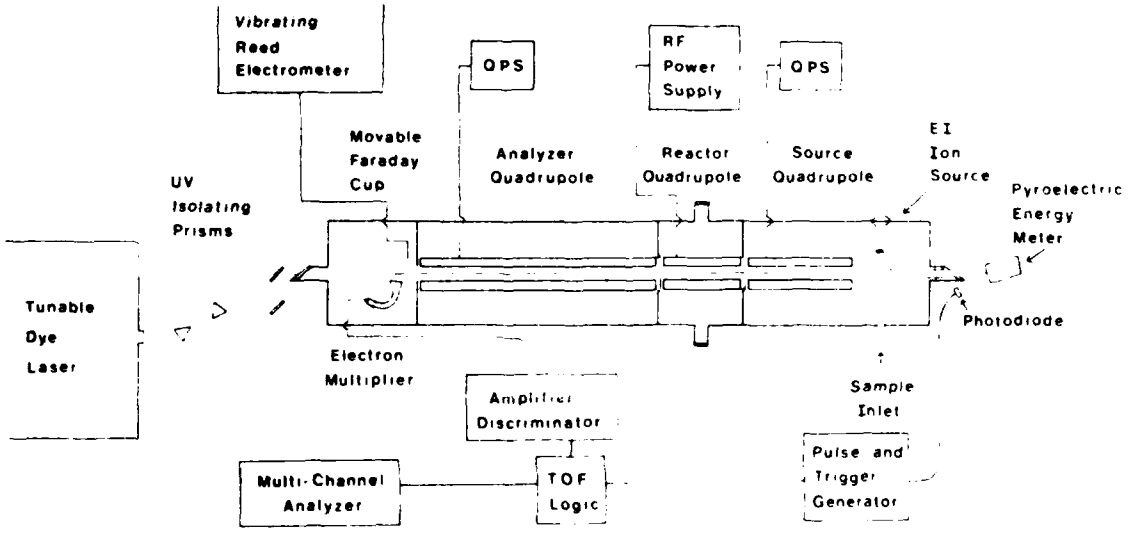

FIG. 2. Schematic diagram of the apparatus. Quadrupole rods are all 1.905 cm in diameter. The rod lengths are: source = 20.32 cm, reactor = 15.24 cm, analyzer = 45.72 cm.

in both the N_2O^+ and SO_2^+ cases, being well onto the plateau shown in Fig. 3 but safely below the low mass cutoff point[22] for any possible products of photodissociation.

The electron impact ion source was commonly operated at a pressure, as measured by an MKS Baratron gauge connected directly to the ionization chamber, of ~ 3 mTorr, with the electrons accelerated through either 50 (for all visible and $\sim\frac{1}{2}$ the UV runs on SO_2^+) or 70 V (for the other UV runs) before entering the ion chamber. The effects of varying source pressure and electron energy on the photodissociation cross sections will be discussed in a subsequent paper. Typical operating pressures in the three quadrupole regions, as read by ionization gauges, were: source $= 8\times10^{-6}$ Torr; reactor $= 7\times10^{-7}$ Torr, and analyzer $= 9\times10^{-8}$ Torr. To provide differential pumping of these regions, the reactor quad was separated from the source quad by 5.1 cm o.d., 0.13 cm thick stainless steel plate containing a 0.318 cm diam centered aperture and from the analyzer quad by a similar plate with a 0.397 cm central aperture. These plates were mounted on Teflon gaskets and connected to dc power supplies and electrometers to focus the ion beam and to measure its transmission through the reactor and/or the analyzer (see below).

Use of the triple quadrupole system increased the effective light path by nearly 50 times and the ion density in the ion–photon interaction region by at least an order of magnitude (for comparable source conditions) compared to the former apparatus.[19] For the test measurements on N_2O^+, however, the yield of photoproduct ions was only increased by a factor of ~ 15 (to ~ 2 NO^+ ions per laser pulse at ~ 3381 Å, $\sim 50\,\mu$J per pulse and $\sim 1\times10^{-9}$ Å of N_2O^+ current). After completing the N_2O^+ cross section measurements and doing 244 SO_2^+ runs, the collection efficiency of the off-axis Channeltron No. 4830 electron multiplier was increased ~ 50 times by inserting a deflection electrode on the other side of the exiting ion beam from the electron multiplier. The optimum collection efficiency was obtained when the potential on this electrode was raised to $+900$ V, and the entrance to the Channeltron was at -2000 V, giving an electric field between the two of $\sim 1.5\times10^5$ V m^{-1}. This greatly improved sensitivity resulted in shorter run times and reduced errors in the ion-counting statistics—especially beneficial when using the weak UV output of the dye laser. It was necessary, in fact, to reduce transmission (by increasing resolution) of the first and third quadrupoles and reduce the emission current in the ion source to avoid saturation effects at the multiplier[21] in some cases. The number of product ions per laser pulse was kept below 10 for $\lambda < 3600$ Å and < 25 for $\lambda > 4400$ Å.

Figure 4 shows the time distribution of photoproduct SO^+ ions following the laser pulse for a wavelength corresponding to one of the peaks found in the visible photodissociation spectrum of SO^+. In this case 13 product ions were formed per laser pulse, above the background count rate of 0.06 ion per pulse, over the time range: 48–294 μs. A brief investigation of the effect of pressure in the reactor quad upon the background SO^+ count rate showed it to be due to the collision-induced dissociation

$$SO_2^+ + M \xrightarrow{k} SO^+ + O + M \qquad (1)$$

with $k \simeq 1\times10^{-11}$ cm^3/s for E_2 (the reactant ion kinetic en-

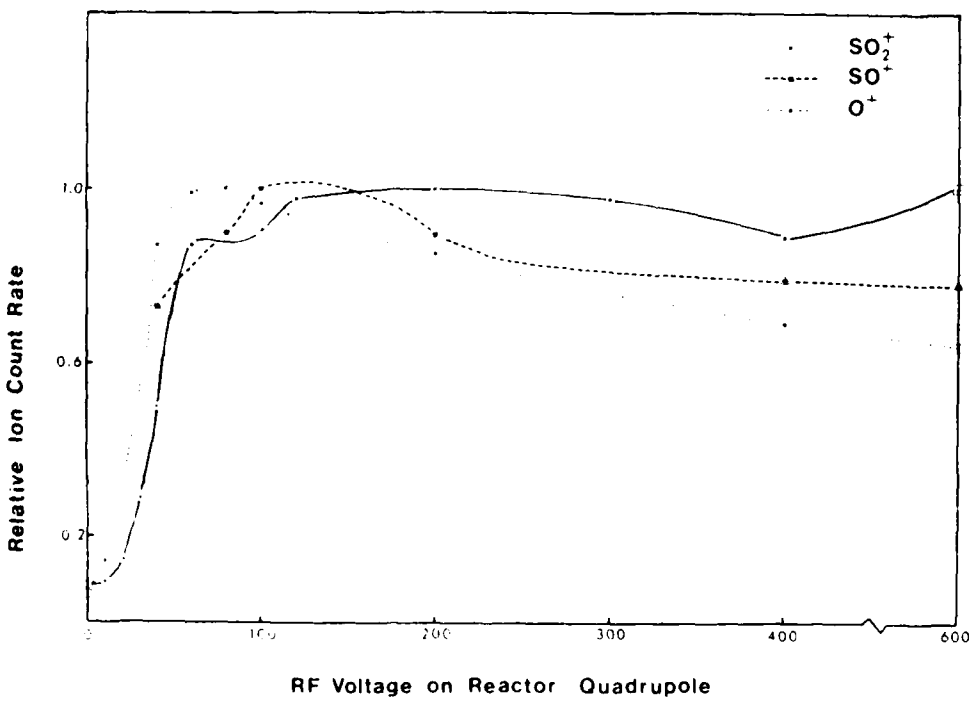

FIG. 3. Effect of rf voltage on ion transmission: rf frequency = 2.1 MHz; E_1 = 27 eV; E_2 = 3.0 eV; E_3 = 32 eV. The source quadrupole selected the indicated ions and the analyzer quadrupole was in the rf-only mode (mass setting = 16 amu).

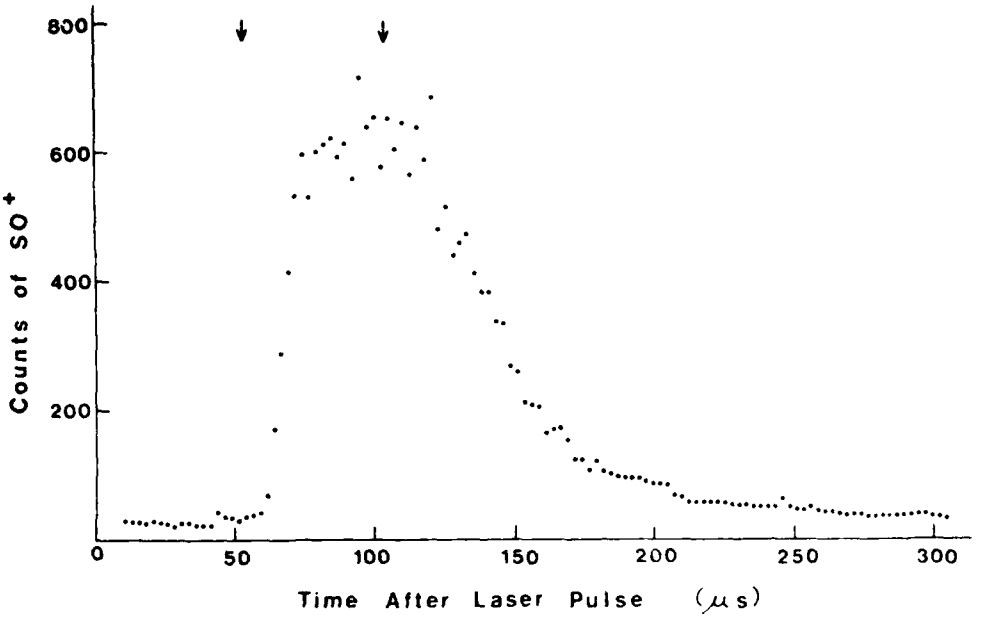

FIG. 4. Time-of-flight spectrum of SO^+ formed from SO_2^+ by λ_{uv} = 4965.1 A. Produced by 1555 laser pulses averaging 202 μJ per pulse. Ion energies: E_1 = 16.0 eV, E_2 = 3.9 eV, E_3 = 20 eV. V_{rf} = 400 VAC, i_{DC} = 6.64×10^{-10} A, T_R = 0.133

ergy) = 2.0–5.0 eV. Here "M" represents background gas plus SO_2 leaking in from the source region.

The small vertical arrows in Fig. 4 indicate the calculated limits on the flight times for SO^+ ions formed at the entrance (second arrow) and exit (first arrow) of the reactor quadrupole, assuming a kinetic energy release of 0.1 eV. The shift of the observed TOF peak to longer times may be partly the result of contact potentials, surface charge, and space charge effects, which usually reduce the actual energy of positive ion beams below the values set on external power supplies. The width of the top of the peak is, however, consistent with E_2 = 3.9 eV; the long tail probably reflects an ion energy spread of several eV. For example, the full width at half-height of the TOF peak corresponds to E_2 = 1.3 eV. Later experiments[23] have suggested that part of this energy spread originates in the ion source and that part is caused by the source quadrupole—perhaps by creating a large angular divergence in the ion beam entering the reactor quadrupole.

The wavelength output of the CMX-4 laser was determined for every cross section measured by diverting a portion of the laser beam via a 20 ft long optical fiber into a 0.5 m scanning monochromator. For $\leq$3600 A the small amount of fundamental coming through the frequency doubling crystals was separated from the UV beam by a pair of second harmonic dispersive prisms (Inrad Model 751-101), as shown in Fig. 2, and directed into the optical fiber. For $\lambda \geq$4360 Å the UV-isolating prism were replaced by a beam splitter which reflected a small fraction of the stronger incident beam into the fiber. The monochromator itself was calibrated daily by scanning appropriate portions of the emission spectra of neon or mercury discharge tubes. The wavelength calibrations were made to an accuracy of $\pm$ 0.1 Å. The monochromator scans of the laser output showed full widths at half-maximum of 0.5–0.9 Å in the UV (3000–3600 Å) and 0.8–1.4 Å in the visible region above 4692 Å. At the blue end of the laser's undoubled output (λ = 4360–4744 Å, using the laser's "A" tuning scale), however, it proved impossible to reduce $\Delta\lambda_{1/2}$ below 10 Å.

Calculation of photodissociation cross sections was modified slightly from the earlier method[19] to reflect the change from transverse to coaxial illumination of the ion beam (see Fig. 5). The previously derived basic equation now becomes

$$\sigma = N_+ eU_p / P_\# \int (i_p I_0 Z / A)\, dX\, dY, \tag{2}$$

where N_+ is the total number of photoproduct ions above the background, e the charge on a primary ion, U_p the axial velocity of the primary ion, $P_\#$ the number of laser pulses, i_p the primary ion current, I_0 the number of photons per unit area per laser pulse, Z the laser beam path length through the interaction region, and A the cross sectional area of the ion beam. All quantities refer to the interaction region within the middle quadrupole. A 1.6 mm aperture, placed in the laser beam just before the entrance window to the triple quadrupole, ensured that the slowly diverging laser beam remained wholly within the ion beam throughout the reactor quadrupole. Since the intensity profile of the ion beam along the X and Y directions could not be determined on our apparatus, i_p was assumed to be independent of X and Y. Integration of Eq. (2) across the interaction region then gives

$$\sigma = hcN_+ eU_p \bar{A} / P_{\#\,p} E_0 \lambda Z, \tag{3}$$

where $\bar{A}$ is the cross sectional area at the midpoint of the interaction region, E_0 is the average energy per laser pulse, and λ is the laser wavelength.

Substitution of known constants and geometric factors yields the working equation

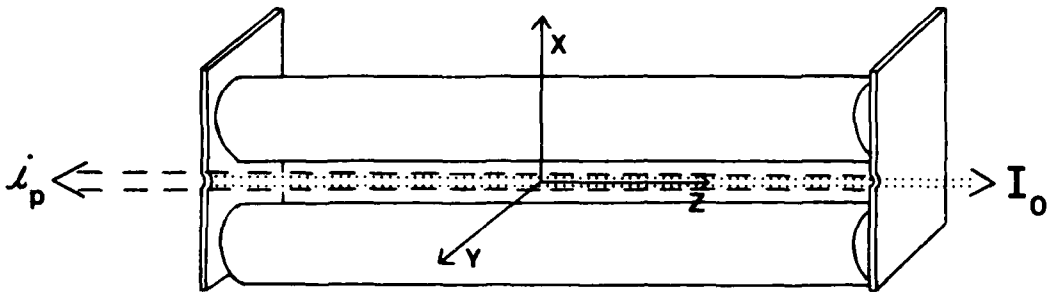

FIG. 5. Photon–ion interaction region. Laser beam enters through 0.397 cm diam aperture on the left and primary ion beam through a 0.318 cm diam aperture on the right.

$$\sigma = \frac{7.206\times10^{-15}[V_p/(3.9)(63.96/M_p)]^{1/2} N_s}{P_\# E_0 \lambda I_p T_R}, \quad (4)$$

in which V_p is the primary ion energy in eV, M_p is the molecular weight of the primary ions, E_0 is in μJ, λ in Å, and I_p—the primary ion current measured at the Faraday cup following the analyzer quadrupole—is in units of 10^{-10} amp. T_R represents the ratio of the transmission of the product ions through the analyzer quadrupole to the electron multiplier to the transmission of primary ions through the analyzer quadrupole to the movable Faraday cup. The transmissions were determined at reduced ion beam currents by sequentially measuring the ion current entering the analyzer quadrupole and then the ion count rate (at the electron multiplier) or current (on the Faraday cup) at the appropriate detector. The ion current entering the analyzer quadrupole was obtained from the change in current striking the 5.1 cm plate separating the second and third quadrupoles when the bias on the analyzer quadrupole rods was switched from its normal setting to ~ 100 V more positive—driving essentially all the ions back onto the divider plate. Since the transmissions depended on many instrumental factors (e.g., ion energy, quadrupole resolution, multiplier voltage, and history), they were determined at least twice each day that a set of cross sections was measured. Values ranged from 0.19–0.60 for transmission of SO_2^+ to the Faraday cup, and from 0.02–0.23 for transmission of SO^+ to the electron multiplier (after installation of the deflection electrode). The resulting T_R values generally fell between 0.1 and 0.5.

III. RESULTS AND DISCUSSION

A. N_2O^+

Since considerable effort had been devoted to obtaining absolute cross sections for photodissociation of N_2O^+ in the 3000–3400 Å region on our former transverse irradiation system, the accuracy of the new system was tested by making another series of measurements of the reaction

$$N_2O^+ + h\nu \rightarrow NO^+ + N. \quad (5)$$

Initially, the measurements of NO^+ yield at a fixed wavelength were used to align the laser beam for maximum overlap with the ion beam and optimize other experimental parameters. Then, several sets of cross sections were determined in the wavelength region previously assigned to the strong $\tilde{A}\,^2\Sigma^+(1,0,0)\leftarrow\tilde{X}\,\Pi_{3/2}(0,0,0)$ transition in N_2O^+.[19] Our experimental results are contained within the rectangular error boxes in Fig. 6. The solid curve represents the best fit to a much more extensive set of data obtained by Rose *et al.*[24] using our previous apparatus. The uncertainty in the wavelength may be larger than indicated (i.e., up to $\pm$ 0.5 Å), since the procedure of daily calibration of the reference monochromator was not begun until after completion of our measurements on N_2O^+, but our peak values of the photodissociation cross sections are in remarkably good agreement with the earlier values.[25] The apparent value of λ_{max} for this transition is also in reasonable agreement with the predicted value (3381.2 Å *in vacuo*, 3380.2 Å in air) and

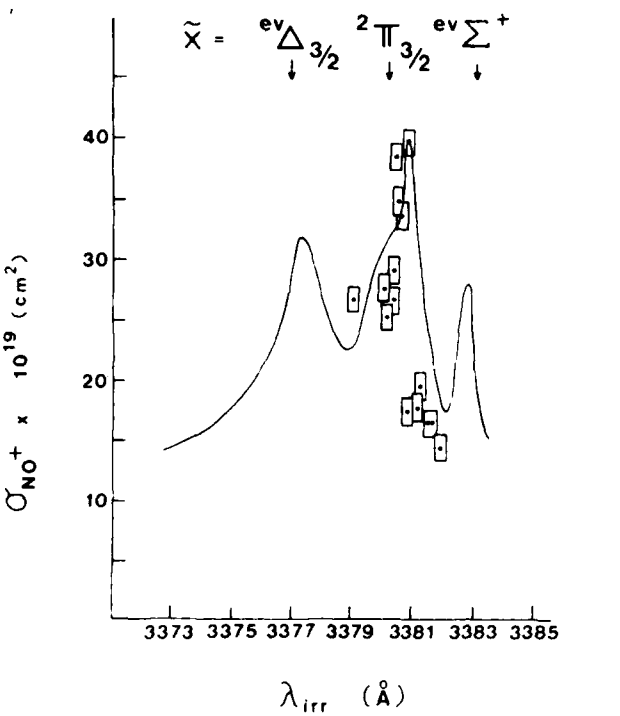

FIG. 6. Photodissociation spectrum of N_2O^+, showing three components of the $\tilde{A}\,^2\Sigma^+(v_2' = 1) \leftarrow \tilde{X}(v_2 = 0)$ transition. The solid curve is from the data of Rose *et al.* (see Ref. 24) and the points within the error boxes are from this work. Wavelengths were calibrated in air. The two transitions bearing the "eV" superscript originate from ions having $v_2 = 1$, leading to the splitting by the Renner effect.

even the hint of a rotational contour is consistent with the recent high resolution results of Abed *et al.*[26]

Since our original report on the photodissociation of N_2O^+, a threshold photoelectron–photoion coincidence study of N_2O found that 1/30 of the fragmentation occurring from the (1,0,0) vibrational levels of the $\tilde{A}\,^2\Sigma$ state of N_2O^+ yields O^+ as product instead of NO^+.[27] Taking advantage of the increased sensitivity of our present apparatus we measured the following product ratios near the 3381 Å peak in the photodissociation spectrum:

$$\frac{\sigma_{O^+}}{\sigma_{NO^+}} = 1.1 \pm 0.1 \times 10^{-2}$$

and

$$\frac{\sigma_{N_2^+}}{\sigma_{NO^+}} = 1.4 \pm 0.3 \times 10^{-3}.$$

The first ratio agrees with Nenner's, within her larger range of uncertainty, and is consistent with our earlier report that $\sigma_{O^+} < 6 \times 10^{-20}$ cm^2 at 3218 Å. The second result presumably indicates the presence of a small concentration of an electronically excited state in the ion beam since Nenner *et al.* observed no N_2^+ formation below the $\tilde{C}\,^2\Sigma^+$ state.[27] This could be the $\tilde{A}\,^2\Sigma^+$ state itself, except that it has a reported lifetime of only 220 ns in the (0,0,0) level[28]—compared with a flight time of 17 μs through our source quadrupole. Thus the N_2^+ formation may result from absorption by a previously undetected quartet state of N_2O^+.[45]

There had also appeared a report of the photodissociation of N_2O^+ by the 4880 Å line of an argon ion laser.[29] Although photodissociation is energetically possible, no electronically excited states are accessible from the $\tilde{X}$ state, at this wavelength. We therefore measured cross sections at several λ's near 4880 Å and obtained the results

$$\sigma_{NO^+} < 1 \times 10^{-20}\ \text{cm}^2; \quad 4880.5\ \text{Å} < \lambda < 4881.3\ \text{Å}$$

and

$$\sigma_{N_2^+} = 4.6 \pm 0.4 \times 10^{-21}\ \text{cm}^2; \quad \lambda_{max} = 4880.1\ \text{Å}.$$

The first result is consistent with our earlier negative results on looking for photodissociation of N_2O^+ in the visible,[19] but not with the report of Carrington *et al.*[29] The second result is more precise because of the lower background count rate for N_2^+ than for NO^+. The source of the small N_2^+ yield may be absorption by the same excited state responsible for the trace of N_2^+ observed for $\lambda_{irr} = 3381$ Å.

B. SO_2^+-visible spectrum

Cross sections for formation of SO^+ by photodissociation of SO_2^+ in the visible region are plotted vs irradiation wavelength in Figs. 7 and 8. Data for $\lambda_{irr} = 4900$–5120 Å

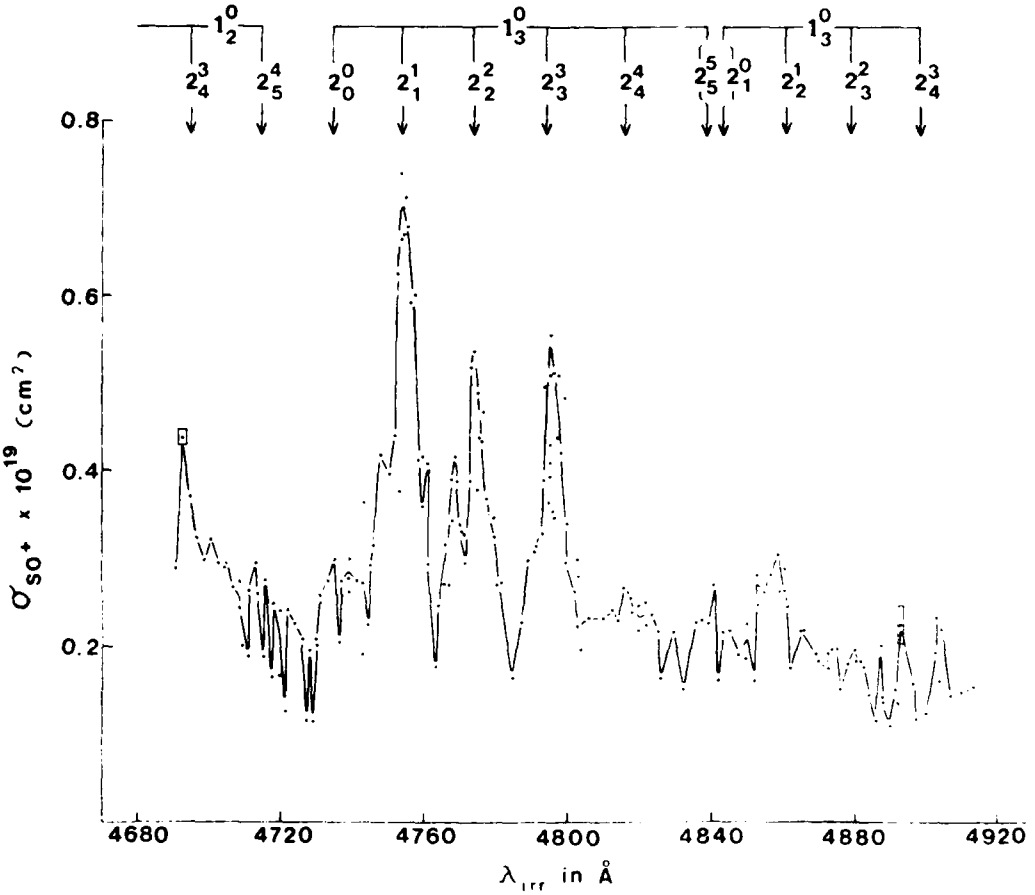

FIG. 7. Photodissociation spectrum for the process $SO_2^+ + h\nu \rightarrow SO^+ + O$. Statistical uncertainty in cross sections and $\Delta\lambda_{irr}$ for the irradiation wavelengths are indicated by rectangles near each end of spectrum. Exciton's laser dye LD-473 was used for full range of this spectrum. The positions of the vertical arrows denoting the major sequences in the spectrum were calculated from the spectroscopic constants in Table II

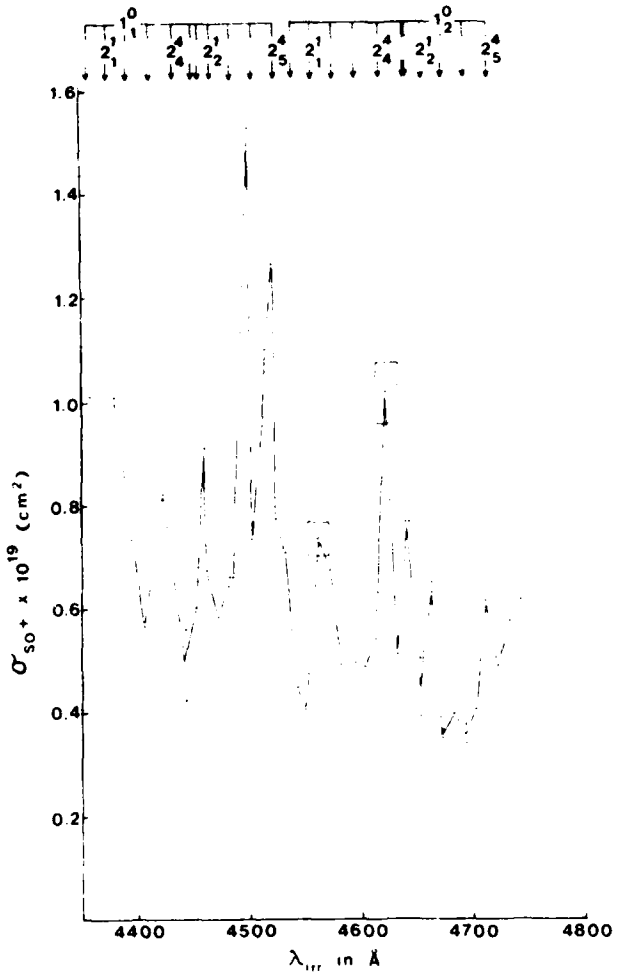

FIG. 8. Photodissociation spectrum for the process $SO_2^+ + h\nu \rightarrow SO^+ + O$. Error rectangles have same meaning as in Fig. 7. Exciton's Coumarin 440 and Coumarin 450 dyes were used for the wavelength range shown. Vertical arrows designate vibrational bands calculated from the constants in Table II.

were shown in a previous communication.[30] To reduce the error contributed by day-to-day variations in the unknown overlap of the laser beam with the ion beam, cross sections were ratioed with ones measured at a fixed reference wavelength. One reference wavelength was selected for each dye used and the absolute cross sections at those wavelengths were averaged over many different days (an average of nine times each). Indicated peaks in the spectrum were usually confirmed by repeated "scans" over the peak tops on separate days. Wavelength intervals between successive measurements of the cross section were typically ~ 2 Å, except in the 4400–4700 Å region where a step size of ~ 10 Å was used because of the broader bandwidth of the laser there.

Table I lists the wavelengths of the photodissociation peaks located in our spectra and the corresponding cross sections. The most pronounced features of our spectra are sequences with separations of 80–90 cm^{-1}. Less obvious (because of the limitations on our wavelength range) but still fairly clear are progressions of 850–910, 720–760, 410–490, and $\sim$ 300–400 cm^{-1}. Based on vibrational frequencies for the ion derived from photoelectron[31,32] and photoionization[33] spectral data for SO_2, the two largest intervals were assigned to the symmetric stretch ($\tilde{\nu}_1''$ and $\tilde{\nu}_1'$ for the lower and upper states, respectively) and the two smallest intervals to the bending mode of the ion ($\tilde{\nu}_2''$ and $\tilde{\nu}_2'$). The observed sequence was then assigned to transitions having $\Delta v_2 = 0$ (most prominent), -1 (next), or $+1$ (weakest). The length of these sequences, to $v = 7$, is consistent with the extensive excitation of the bending mode of the ion seen in the first two bands of the photoelectron spectrum of SO_2.[31,34] There is no indication of transitions involving ν_3 either in our spectra or in the PES and PI of SO_2.

The vibrational energy (in cm^{-1}) of a nonlinear triatomic ion in a given electronic state may be represented by [35]

$$T_{vib} = \sum_{k=1}^{3} (v_k + \tfrac{1}{2})\tilde{\nu}_k + \sum_{i=1}^{3}\sum_{k\geq i}^{3} X_{ik}(v_i + \tfrac{1}{2})(v_k + \tfrac{1}{2}). \quad (6)$$

Here $\tilde{\nu}_k$ = fundamental vibrational frequency of mode k, v_k = vibrational quantum number for that mode, and X_{ik} = anharmonicity constant.

The separation of adjacent peaks in a progression in v_2'' is

$$\begin{aligned} &T_{vib}(v_1'', v_2'' + 1) - T_{vib}(v_1'', v_2'') \\ &\quad = \lambda^{-1}(v_1'', v_2'' + 1 \rightarrow v_1', v_2') \\ &\qquad - \lambda^{-1}(v_1'', v_2'' \rightarrow v_1', v_2'), \end{aligned} \quad (7)$$

and, from Eq. (6)—assuming $v_3'' = v_3' = 0$ and $X_{23} = 0$:

$$\begin{aligned} &T_{vib}(v_1'', v_2'' + 1) - T_{vib}(v_1'', v_2'') \\ &\quad = \tilde{\nu}_2'' + X_{12}''(v_1'' + \tfrac{1}{2}) + 2X_{22}''(v_2'' + 1). \end{aligned} \quad (8)$$

Similarly, for progressions in v_1'':

$$\begin{aligned} &T_{vib}(v_1'' + 1, v_2'') - T_{vib}(v_1'', v_2'') \\ &\quad = \tilde{\nu}_1'' + X_{12}''(v_2'' + \tfrac{1}{2}) + 2X_{11}''(v_1'' + 1). \end{aligned} \quad (9)$$

Equations of the same form may be fit to the progressions in v_1' and v_2'.

In order to assign the vibrational quantum numbers to the peaks it was necessary to locate λ_{00} for the transitions occurring in the visible region. Our previous communication[30] showed that the transition originates in a metastable state having a lifetime of $\sim 25 \times 10^{-6}$ s, for $\lambda_{irr} = 4965$ Å. Recent theoretical calculations on SO_2[36–38] appear to be in unanimous agreement that the second ionization potential corresponds to formation of SO_2^+ in the $^2A_2$ state, as shown in Fig. 1. Since radiative decay of this state to the ground state is forbidden in C_{2v} symmetry, it seems to be the most likely origin of the observed transitions. The data of Eland and Danby[31] show and the calculations of Cederbaum *et al.*[38] predict that both $\tilde{\nu}_1$ and $\tilde{\nu}_2$ should be significantly excited—with up to ~ 0.6 eV of total vibrational energy—when the $^2A_2$ state is initially formed.

The vibrational quantum numbers assigned to the observed peaks, assuming only ν_1 and ν_2 are involved in the transitions and that the transitions originate in the $\tilde{A}\,^2A_2$ state, are shown in the fourth column of Table I. Progressions in v_2 are plotted as a function of v_2'' (upper two lines) and

TABLE I. Observed peaks.

λ_{exp} (Å), in air	$\Delta\lambda$ (Å)	λ_{calc} (Å)	Transition	$10^{19}\times\sigma_{SO_2}$ (cm^2)
5112	1.0	5115.1	$1_3^0\,2_2^3$	0.14
		5112.6	$1_3^1\,2_2^1$	
5103.1	2.0	5107.6	$1_4^0\,2_7^7$	0.16
5096	1.0	5097.9	$1_4^0\,2_3^2$	0.14
5080	2.0	5080.0	$1_4^0\,2_2^1$	0.12
		5079.2	$1_4^0\,2_6^6$	
5065	2.0	5063.9	$1_4^0\,2_1^0$	0.12
5052	2.0	5052.7	$1_4^0\,2_5^5$	0.12
5047	2.0	...	?	0.12
5028	2.0	5028.1	$1_4^0\,2_4^4$	0.19
5019.8	1.0	5017.5	$1_3^1\,2_2^2$	0.17
5012	2.0	5007.4	$1_3^1\,2_5^6$	0.19
5003	1.0	5005.4	$1_4^0\,2_3^3$	0.24
		5002.1	$1_4^0\,2_4^7$	
4985.2	1.0	4984.5	$1_4^0\,2_2^2$	0.28
4979.2	1.0	4980.2	$1_3^1\,2_0^0$	0.21
		4976.6	$1_4^1\,2_6^5$	
4966	1.0	4965.3	$1_4^0\,2_1^1$	0.25
4951.4	1.0	4953.3	$1_4^1\,2_5^4$	0.16
4948	1.0	4947.8	$1_4^0\,2_0^0$	0.17
4945	2.0	4945.4	$1_4^0\,2_4^5$	0.17
		4942.4	$1_3^0\,2_6^3$	
4935.4	2.0	4931.7	$1_4^1\,2_4^3$	0.18
4919.6	1.0	4919.8	$1_4^0\,2_3^4$	0.21
		4919.4	$1_3^0\,2_5^4$	
4910.2	1.0	4911.9	$1_4^1\,2_5^5$	0.18
4903.5	1.0	4900.5	$1_4^1\,2_6^6$	0.23
		4898.2	$1_3^0\,2_4^4$	
4893	2.0	4893.8	$1_4^1\,2_2^1$	0.23
		4893.4	$1_3^0\,2_7^7$	
4887.4	1.0	4886.4	$1_3^1\,2_0^1$	0.20
4880.0	1.0	4878.7	$1_3^0\,2_3^2$	0.20
4874.8	2.0	4874.4	$1_4^1\,2_5^5$	0.20
		4874.0	$1_4^0\,2_1^2$	
4865.3	2.0	4865.9	$1_3^0\,2_6^6$	0.22
4858.8	2.0	4860.9	$1_3^0\,2_2^1$	0.30
4852.8	1.0	4853.7	$1_4^0\,2_0^1$	0.27
		4850.1	$1_4^1\,2_4^4$	
4842.4	2.0	4844.7	$1_3^0\,2_1^0$	0.22
4841.0	1.0	4840.2	$1_3^0\,2_5^5$	0.27
4829.6	2.0	4827.4	$1_4^1\,2_3^3$	0.22
4816.0	1.0	4816.2	$1_3^0\,2_4^4$	0.27
4795.0	1.0	4794.0	$1_3^0\,2_3^3$	0.55
4774.0	1.0	4773.4	$1_3^0\,2_2^2$	0.53
4768.5	0.5	4769.6	$1_4^1\,2_0^0$	0.42
		4766.8	$1_3^0\,2_5^5$	
4761.0	0.5	4761.5	$1_3^0\,2_7^7$	0.41
4754.0	1.0	4754.4	$1_3^0\,2_1^1$	0.72
4747.8	1.0	4748.8	$1_3^1\,2_5^4$	0.42
4739	2.0	4740.2	$1_3^1\,2_4^5$	0.29
4735.1	1.0	4737.4	$1_3^0\,2_6^5$	0.30
		4737.0	$1_3^0\,2_0^0$	
4713.5	1.0	4715.4	$1_3^0\,2_3^4$	0.29
		4714.9	$1_3^0\,2_4^4$	
4700.3	1.0	4701.7	$1_3^1\,2_6^6$	0.32
4692.6	1.0	4694.1	$1_3^1\,2_4^4$	0.44
		4693.7	$1_3^0\,2_5^5$	
		4692.2	$1_3^0\,2_2^2$	
		4690.1	$1_3^1\,2_2^1$	
4683	10	4683.4	$1_4^1\,2_6^5$	0.40
		4676.3	$1_3^1\,2_5^5$	
		4674.9	$1_3^0\,2_5^5$	

TABLE I (*continued*).

λ_{exp} (Å), in air	$\Delta\lambda$ (Å)	λ_{calc} (Å)	Transition	$10^{19} \times \sigma_{SO_2^+}$ (cm^2)
4663	5	4667.1	$1_2^0 2_6^6$	0.65
4642	5	4642.1	$1_2^0 2_5^5$	0.77
		4641.0	$1_2^0 2_1^0$	
4623	6	4618.7	$1_2^0 2_4^4$	1.02
4595.5	8	4597.0	$1_2^0 2_3^3$	0.50
4562	10	4558.0	$1_2^1 2_5^5$	0.74
		4558.0	$1_2^0 2_1^1$	
4521	5	4524.2	$1_1^0 2_5^4$	1.26
		4518.0	$1_2^1 2_3^2$	
4500	8	4507.1	$1_1^0 2_7^7$	1.56
		4503.7	$1_1^0 2_4^3$	
		4500.2	$1_2^1 2_2^1$	
4460	5	4468.0	$1_2^1 2_4^4$	0.91
		4467.3	$1_1^0 2_2^1$	
		4457.1	$1_1^0 2_5^5$	
4423	10	4426.3	$1_2^1 2_5^5$	0.82
		4424.5	$1_1^1 2_7^6$	
4370	13	4374.9	$1_1^0 2_1^1$	>1.02
		4369.8	$1_1^0 2_4^5$	
		4367.1	$1_1^1 2_7^7$	

of v_2' (lower line) in Fig. 9. All but one of the experimental points lie on the least squares straight lines within the estimated experimental errors in $\Delta\lambda^{-1}$—the larger values of which result from including peaks observed in the troublesome 4400–4700 Å region. From Eq. (8) and its analog for the upper electronic state the slopes of these lines gave values for X'_{22} and X''_{22}. To obtain $\tilde{\nu}_2$'s from the intercepts it was then necessary to derive values for X'_{12} and X''_{12}. This was done by plotting the progressions in v_1 as a function of v_2 as shown in Fig. 10, and using Eq. (9). To obtain $\tilde{\nu}_1''$, the intercepts from Fig. 10 were corrected by $\frac{1}{2}X''_{12}$ and the set of equations

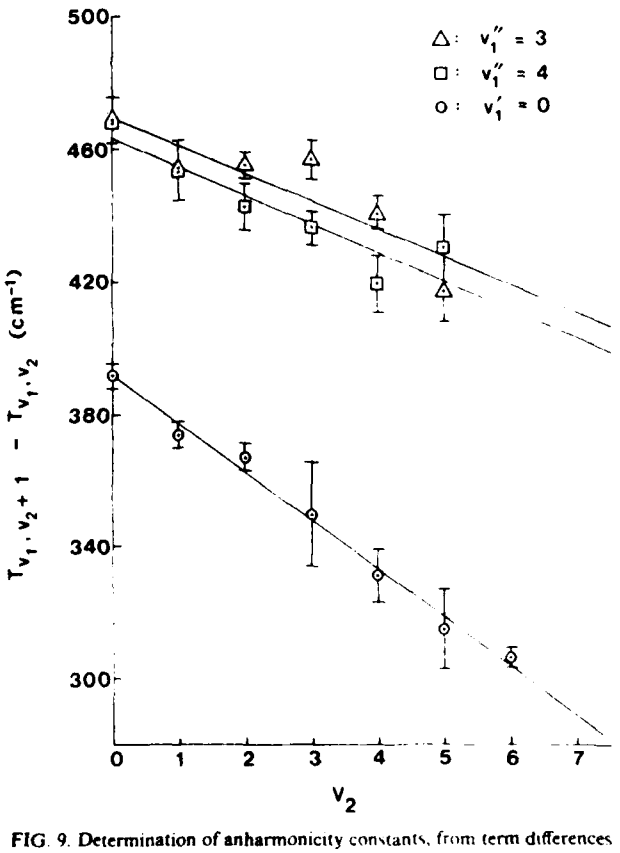

FIG. 9. Determination of anharmonicity constants, from term differences ($\Delta v_2 = +1$) derived from the photodissociation spectrum of SO_2^+ between 4400–5120 Å. For the upper two lines: $v_2 = v_2''$, for the lowest line: $v_2 = v_2'$.

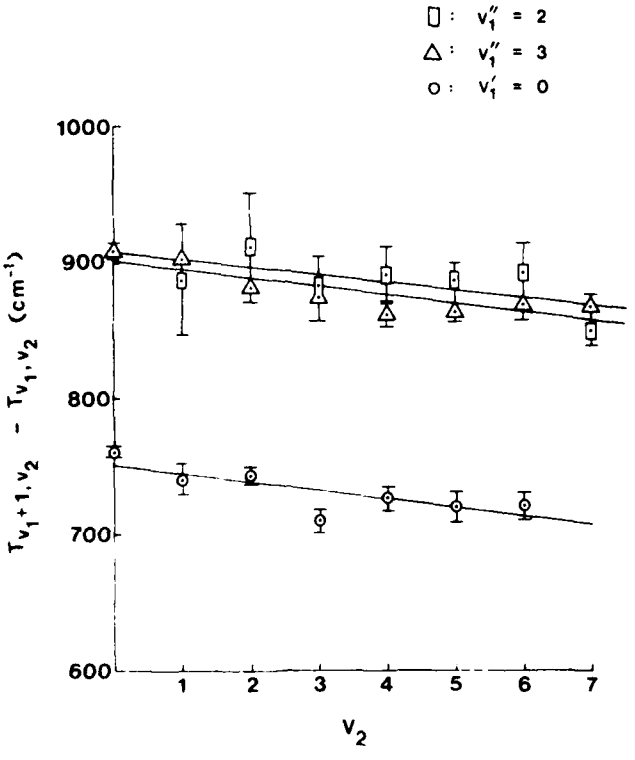

FIG. 10. Determination of anharmonicity constants from term differences ($\Delta v_1 = +1$). For the upper two lines: $v_2 = v_2''$; for the lowest line: $v_2 = v_2'$.

$$T_{vib}(v_1'' + 1, v_2'' = 0) - T_{vib}(v_1'', v_2'' = 0) - \tfrac{1}{2}X''_{12} = \tilde{\nu}_1'' + 2X''_{11}(v_1'' + 1)$$

was solved simultaneously for ν_1'' and X''_{11}. In addition to the data from our photodissociation spectrum the value

$$T_{vib}(v_1'' = 1, v_2'' = 0) - T_{vib}(v_1'' = 0, v_2'' = 0) = 934.9\ \text{cm}^{-1}$$

was taken from the IR photodissociation peak found in SO_2^+ by Kompa *et al.*[39] Insufficient data on progressions in v_1' prevented experimental determination of X'_{11}.

The vibrational frequencies and anharmonicity constants derived as described above are presented in Table II. The difference in T_0 (electronic energy plus zero point vibrational energy) for the two states was adjusted for best fit to all the peaks shown in Table I; it corresponds to $\lambda_{00} = 4187$ Å. Since completing the analysis of our data, we have learned that Goss, McLoughlin, and Morrison[40] recently observed a peak at 4187.0 Å in the photodissociation spectrum of SO_2^+. They have assigned their observed spectrum to the transition $\tilde{C} \leftarrow \tilde{B}$, with $\lambda_{00} = 4555.4$ Å, but the fit to their data was not sufficiently good to yield anharmonicity constants. The three vibrational frequencies which they extracted from their spectra are compared with our values in Table II. The lack of correction for anharmonicity should make their values significantly smaller than ours (see Figs. 9 and 10).

The calculated transition wavelengths shown in column three of Table I were obtained using our spectroscopic constants from Table II and setting all unknown anharmonicity constants equal to zero. The unknown antisymmetric stretching frequencies were taken to be $\tilde{\nu}_3'' = 1127\ \text{cm}^{-1}$ and $\tilde{\nu}_3' = 892\ \text{cm}^{-1}$, based on the ratio $\tilde{\nu}_3/\tilde{\nu}_1 = 1.183$ found in neutral SO_2.[41] The mean absolute deviation between our calculated and observed transition wavelengths is 1.5 Å in the 4693–5112 Å range and 3.6 Å for $\lambda = 4370$–4683 Å. The uncertainty indicated in Table II for T_0 of the $\tilde{A}$ state corresponds to the smaller of these deviations, taking the indicated T_0 for the $\tilde{C}$ state to be exact.

C. SO_2^+-UV spectrum

Cross sections for SO^+ formation in the ultraviolet region are plotted vs irradiation wavelength in Fig. 11. Because the reduced laser output in this region (10–75 μJ/pulse) required a much larger number of laser pulses to get good ion counting statistics, a step size of 4 Å was routinely used in this region. Near expected peaks in the progressions in v_1' and v_2', and especially near the expected value of $\lambda_{(\infty)}$ for the $\tilde{C} \leftarrow \tilde{X}\ ^2A_1$ transition, many repeated scans were made at smaller wavelength intervals ($\lesssim 2$ Å). The positions of the arrows above the spectrum were calculated using Eland and Danby's[31] values for the first and fourth ionization potentials of SO_2 and our values for $\tilde{\nu}_1$, $\tilde{\nu}_2$, X_{11}, X_{12}, and X_{22} in the $\tilde{C}$ state of SO_2^+ (see Table II). Although there is an approximate correspondence between the arrow locations and broad features in the spectrum, the lack of clearly resolved peaks precluded a detailed vibrational analysis.

We interpret the lack of clearly resolvable vibrational structure in Fig. 11 to be the result of a severe congestion of transitions of our vibrationally and rotationally hot ions. If $\nu_2'' = 403\ \text{cm}^{-1}$ for the $\tilde{X}\ ^2A_1$ state of SO_2^+,[31] the expected sequences in $\tilde{\nu}_2$ (corresponding to $\Delta v_2 = 0$, for instance) for the $\tilde{C} \leftarrow \tilde{X}$ transitions would have a separation of $< 10\ \text{cm}^{-1}$ or ~ 1 Å—slightly larger than the UV bandwidth of the laser but probably less than the rotational width of the peaks, as indicated by Fig. 7. The photoelectron spectrum of SO_2 shows that excitation up to $v_2 = 10$ accompanies formation of SO_2^+ in the $\tilde{X}\ ^2A_1$ state.[41] Thus the unresolved sequences in $\tilde{\nu}_2$ should produce bands of 10–→ > 20 Å width, depending on the values of v_2 and the (unknown) anharmonicity constants in the $\tilde{X}$ state. In fact, using the same range of quantum numbers as needed to fit our $\tilde{C} \leftarrow \tilde{A}$ spectrum—$\Delta v_2 = 0, \pm 1$; $v_2 = 0$–→7; but only $\Delta v_1 = 0, +1$ and $v_1 = 0, 1$—we calculate that 152 vibrational peaks lie in the 3100–3400 Å region.

There may also be some overlap with the trailing edge of the $\tilde{C} \leftarrow \tilde{A}$ band [we have some evidence for a peak at 3580 ± 10 Å, which would fit a $1_0^5\,2_0^1$ transition, but very weak laser output (< 5 μJ/pulse) above 3400 Å prevented making a definite assignment]. Both the $\tilde{D} \leftarrow \tilde{A}$ transition, predicted to have $\lambda_{(0)} = 3730$ Å, and the $\tilde{E} \leftarrow \tilde{A}$, $\lambda_{(0)} \simeq 3553$ Å, should also extend into the region spanned by Fig. 11. The radiative transition from the $\tilde{A}\ ^2A_2$ state to a $^2A_1$ state would be symmetry forbidden but, as proposed below, the symmetry assignments shown for the $\tilde{D}$ and $\tilde{E}$ states in Fig. 1 should probably be changed. In any case, the smaller cross sections

TABLE II. Spectroscopic constants for SO_2^+.

	$\tilde{A}$ ($^2A_2$) state		$\tilde{C}$ state	
	This work	Literature	This work	Literature
$\tilde{\nu}_1$ (cm^{-1})	953 ± 8	1090,[a] 935[d]	767 ± 8	782,[c] 816,[e] 807[c]
$\tilde{\nu}_2$ (cm^{-1})	499 ± 8	403,[a] 380,[c] 488[e]	409.8 ± 2.7	363,[c] 375[e]
X_{11} (cm^{-1})	− 6.3 ± 2.9		− 6.5[f]	
X_{22} (cm^{-1})	− 4.25 ± 1.0		− 7.4 ± 0.3	
X_{12} (cm^{-1})	− 6.1 ± 0.5		− 6.3 ± 2.2	
T_0 (cm^{-1})	5805 ± 7	5686[g] ± 403	29 689[g]	29 689[g] ± 84

[a] Reference 31.
[b] Reference 32.
[c] Reference 34.
[d] Reference 39.
[e] Reference 40.
[f] Assumed, using $X_{11}/X_{12} = 1.03$ from $\tilde{A}$ state values.
[g] Assumed.

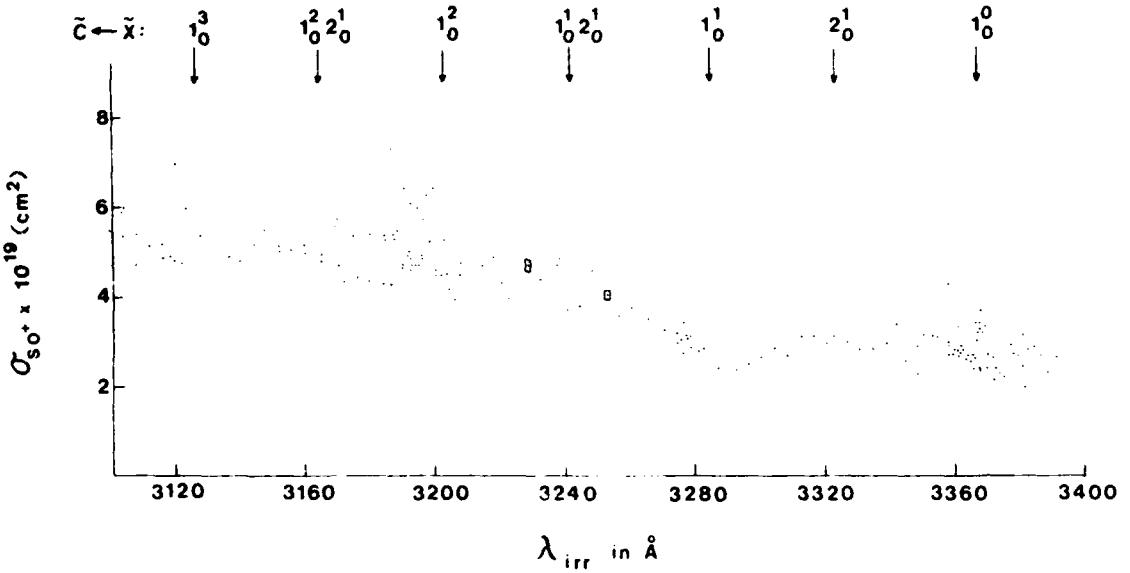

FIG. 11. Photodissociation spectrum for the process $SO_2^+ + h\nu \rightarrow SO^+ + O$. Error rectanges shown near 3228 and 3252 Å have the same meaning as in Fig. 7. Dye solutions used: Rhodamine 6G in aqueous solution with 4% Ammonyx LO; Kiton Red in aqueous solution with 4% Ammonyx LO; Rhodamine 640 in 50:50 methanol + H_2O ($pH \sim 3.5$).

shown in Figs. 7 and 8, compared with Fig. 11, reflect the decay of the population of the $\tilde{A}$ state between the ion source and the photodissociation region to an average of 15% of its initial value, for the operating parameters shown in Fig. 4 and $\tau = 25$ μs. Thus transitions originating in the $\tilde{A}$ state may make only a small contribution to the UV photodissociation spectrum.

According to the threshold photoelectron-coincident photoion experiments of Weiss *et al.*[18] S^+ begins to be formed (in addition to SO^+) from SO_2^+ at a photon energy 4.029 eV above the first ionization potential of 12.305 eV,[31] which would correspond to 3077 Å for a transition originating from the (000) vibrational level of the $\tilde{X}$ state of SO_2^+. They identified this onset with formation of the (310) level in the $\tilde{C}$ state of SO_2^+. At 4.369 eV above the first ionization potential, corresponding to $\lambda = 2838$ Å in our experiment, they reported that S^+ was no longer an observable product.

We searched for S^+ production by direct photodissociation of SO_2^+ over the 3000–3180 Å region and obtained the results shown in Fig. 12. The rather large error bars shown result from the relatively low yield of S^+—never more than ~5% of the SO^+ produced—and from a significant background count rate at mass 32 in our time-of-flight spectra (probably due to efficient charge exchange with background O_2 as well as collision induced decomposition of SO_2^+). In spite of the large error bars there appears to be better defined vibrational structure in the photodissociation spectrum for S^+ (lower trace) than in the accompanying spectrum for SO^+ formation (upper trace). The locations of the peaks do not agree well with the predicted wavelengths for $\tilde{C} \leftarrow \tilde{X}$ transitions, shown by the upper row of vertical arrows in the figure.

The simplest explanation for the onset of S^+ formation coincident with the appearance of vibrational structure appears to us to be that a new electronic transition becomes accessible in this region. A tentative assignment of the main features in Fig. 12, shown by the lower row of vertical arrows, yields the approximate vibrational frequencies: $\tilde{\nu}_2'' = 454 \pm 100$ cm^{-1}, $\tilde{\nu}_1' = 955 \pm 45$ cm^{-1}, $\tilde{\nu}_2' = 411 \pm 60$ cm^{-1}. The first two values agree, within the large indicated uncertainties, with frequencies reported for the $\tilde{X}$ ($\tilde{\nu}_2 = 403$ cm^{-1})[31] and $\tilde{D}$ ($\tilde{\nu}_1 = 936$ cm^{-1})[32] states of SO_2^+, respectively; $\tilde{\nu}_2$ has not previously been determined for the $\tilde{D}$ state. We conclude that $\lambda_{00} = 3108 \pm 4$ Å marks the origin of the $\tilde{D} \leftarrow \tilde{A}$ transition, accompanied by weak S^+ formation.

D. Nature of electronic states involved in photodissociation of SO_2^+

The symmetry identification of states $\tilde{C}$ through $\tilde{E}$ shown in Fig. 1 was based on the observation by Lloyd and Roberts[32] of a progression in $\tilde{\nu}_2$ only in the first part of the "third band" of the photoelectron spectrum of SO_2. Their assignment followed from the *ab initio* SCFMO calculations of Hillier and Saunders[37] which had shown that the $^2B_2$ state resulting from loss of an electron from the $4b_2$ molecular orbital would have the greatest change in equilibrium bond angle ($-10.7°$) from neutral SO_2. However, the same calculations support the hypothesis that S^+ formation via the reaction

$$SO_2^+ + h\nu \rightarrow S^+ + O_2$$

is facilitated by the reduced OSO bond angle and reduced O–O antibonding character in the $^2B_2$ state. Brehm *et al.*[16] have previously used symmetry correlation rules to argue that S^+ can be formed only from the $^2B_2$ state of SO_2^+.[42]

In addition, the relatively large value for $\tilde{\nu}_1$ derived from Fig. 12 for the $\tilde{D}$ state indicates it is formed by removing an

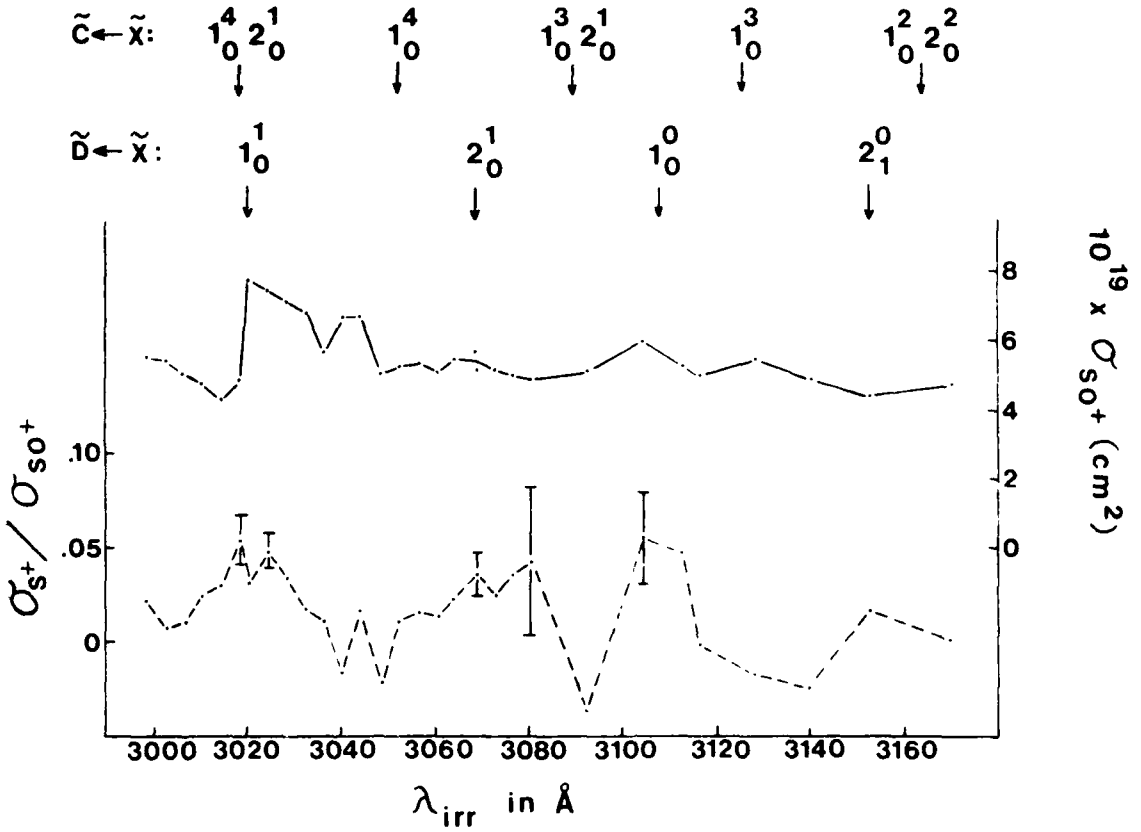

FIG. 12. Branching ratio spectrum for photodissociation of SO_2^+. The lower trace gives the ratio of cross sections for the processes $SO_2^+ + h\nu \rightarrow SO^+ + O$ and $SO_2^+ + h\nu \rightarrow S^+ + O_2$ and the upper trace gives the absolute cross sections for the first process. The error bars represent the combined effect of statistical uncertainties in SO^+ and S^+ ion counts. $\Delta\lambda_{1/2} = 0.5$–$0.9$ Å for the laser this range. Dye solutions used: Rhodamine 6G in 50:50 methanol + H_2O and in 4% Ammonyx LO; and Kiton Red in 4% Ammonyx LO.

electron from a weakly bonding MO such as $4b_2$ rather than the strongly S–O bonding $7a_1$ or $2b_1$.[37,42]

Following the above line of reasoning we conclude that the $\tilde{D}$ state is of $^2B_2$ symmetry, formed by removal of an electron from the $4b_2$ MO. The $\tilde{C}$ state is then probably of $^2B_1$ symmetry, formed by ionization from the $2b_1$ (π_{xo}) orbital, consistent with the smaller $\tilde{\nu}_1 = 767$ cm^{-1}. The small predicted change in equilibrium bond angle ($-2.6°$) for this state is consistent with the short progression ($\Delta v_2 = 0 \rightarrow 1$) in the bending mode observed in the third band of the photoelectron spectrum of SO_2.[32] The failure to observe a progression in the bending mode at energies above the onset of $\tilde{D}$ state formation is understandable in view of the highly congested spectrum and a stated PES solution ranging between 24 and 80 cm^{-1}.

Dujardin and Leach[15] previously suggested that S^+ formation accompanies the onset of the $\tilde{D}$ state in SO_2^+. Our reassignment of this state to $^2B_2$ symmetry, instead of their $^2A_1$, avoids the violation of correlation rules which required them to invoke a "roelectronic induced heterogeneous predissociation" mechanism for S^+ formation. Our interpretation is more easily reconciled with a fast predissociation which limits fluorescence from the $\tilde{D}$ state to $\phi_f \sim 6 \times 10^{-5}$.[15]

IV. CONCLUSIONS, AND SUGGESTIONS FOR FURTHER STUDY

We measured absolute photodissociation cross sections of SO_2^+ in the UV (3000→3400 Å) and the visible (4400–5120 Å). The visible photodissociation spectrum has been assigned to the $\tilde{C}\,^2B_1 \leftarrow \tilde{A}\,^2A_2$ electronic transition and its rich vibrational structure has been analyzed to obtain two harmonic vibrational frequencies ($\tilde{\nu}_1$ and $\tilde{\nu}_2$) and several anharmonicity constants for each state. Attempts to resolve the more highly congested vibrational structure of the UV photodissociation spectrum, thought to correspond principally to the transition: $\tilde{C}\,^2B_1 \leftarrow \tilde{X}\,^2A_1$, were unsuccessful except near the origin of the spectrum for S^+ production. It was proposed that the onset of this process marks the origin of the $\tilde{D}\,^2B_2 \leftarrow \tilde{X}\,^2A_1$ transition and values for $\tilde{\nu}_1$ and $\tilde{\nu}_2$ in the $\tilde{D}$ state were estimated.

A number of future experiments should be considered to test our conclusions and extend (or refine) our results. To confirm the symmetries of our assigned states for the visible photodissociation spectrum, a rotational analysis should be carried out around our proposed origin at 4187 A as well as around Goss, McLoughlin, and Morrison's suggested $\lambda_{(0,0)} = 4555$ A. To do this will require a laser with a much

narrower bandwidth than ours possibly combined with the Doppler-tuning techniques.[26,43] Independent determination of the fundamental vibrational frequencies in the metastable $^2A_2$ state of SO_2^+ could possibly be made by the method of velocity modulation infrared spectroscopy.[44] Accurate values for these frequencies in the $\tilde{X}\,^2A_1$ state would be an aid to analysis of the UV photodissociation spectrum. To resolve the overlapping vibrational structure in the UV spectrum will require both a laser with a narrower bandwidth than ours and a means of reducing the levels of vibrational and rotational excitation of the SO_2^+ ions. Emission studies have not been of any value previously since the combined emission yield of the $\tilde{C}$, $\tilde{D}$, and $\tilde{E}$ states has been estimated to be $\sim 4\times 10^{-5}$.[15] Vibrational constants for the $\tilde{X}$ and $\tilde{B}\,^2B_2$ states of SO_2^+ could be determined, however, if the emission spectrum for $\tilde{B}\rightarrow\tilde{X}$, predicted to have $\lambda_{00} = 13\,190$ Å or $\tilde{\nu}_{00} = 7582\ \mathrm{cm}^{-1}$ could be measured. The results would give further evidence on the question of whether our visible photodissociation originates from the $\tilde{A}$ state as we have concluded or from the $\tilde{B}$ state as proposed by Goss, McLoughlin, and Morrison.[40]

ACKNOWLEDGMENTS

The experimental work reported here was carried out at the Air Force Geophysics Laboratory. Support by Air Force Systems Command Contract No. F19628-84-K-0038 during the subsequent period of manuscript preparation is gratefully acknowledged.

[1] E. C. Y. Inn and J. F. Vedder, Geophys. Res. Lett. **8**, 5 (1981).
[2] J. Heicklen, *Atmospheric Chemistry* (Academic, New York, 1976), pp. 10 and 99.
[3] E. E. Ferguson, F. C. Fehsenfeld, and D. L. Albritton, in *Gas Phase Ion Chemistry*, edited by M. T. Bowers (Academic, New York, 1979), pp. 57–60.
[4] A. J. Krueger, Science **220**, 1377 (1983).
[5] J. M. Rosen, J. Appl. Meteorol. **10**, 1044 (1971).
[6] B. W. Gandrud and A. L. Lazrus, Geophys. Res. Lett. **8**, 21 (1981).
[7] A. A. Viggiano and F. Arnold, Geophys. Res. Lett. **8**, 583 (1981).
[8] F. Arnold and Th. Bührke, Nature **301**, 293 (1983).
[9] Such as HSO_3^+, $H_3SO_4^+$ and $H_3SO_4^+\cdot H_2O$ whose $m/z = 81$, 99, and 117 closely match pronounced peaks found by balloon-borne mass spectrometers at $\sim$35 km. The previously suggested identifications for these peaks, $H^+Y(H_2O)_n$, where Y = CH_3CHO or CO_2 by Arijs (see Ref. 10); and $H^+CH_3NO_2(H_2O)_n$ or $Na^+NaOH(H_2O)_n$ by Arnold and Henschen (see Ref. 11), have not yet been verified.
[10] E. Arijs, D. Nevejans, and J. Ingels, J. Atmos. Terr. Phys. **44**, 43 (1982).
[11] F. Arnold and G. Henschen, Planet. Space Sci. **30**, 101 (1982).
[12] F. Arnold and G. Henschen, Nature **275**, 521 (1978).
[13] A. A. Viggiano, R. A. Perry, D. L. Albritton, E. E. Ferguson, and F. C. Fehsenfeld, J. Geophys. Res. **85**, 4551 (1980).
[14] E. Arijs, D. Nevejans, P. Frederick, and J. Ingels, Geophys. Res. Lett. **8**, 121 (1981).
[15] G. Dujardin and S. Leach, J. Chem. Phys. **75**, 2521 (1981).
[16] R. Brehm, J. H. D. Eland, R. Frey, and A. Kustler, Int. J. Mass Spectrom. Ion Phys. **12**, 197 (1973).
[17] Photodissociation cross sections of SO_2^+ had previously been measured at four wavelengths between 2900 and 3200 Å, under low resolution: R. C. Dunbar, Tech. Report No. AFGL-TR-80-2070 (1980). $\sigma_{SO_2^+} \simeq 5.8\times 10^{-19}\ \mathrm{cm}^{-2}$ was found at both 3000 and 3100 Å.
[18] M. J. Weiss, T. C. Hsieh, and G. G. Meisels, J. Chem. Phys. **71**, 567 (1979).
[19] T. F. Thomas, F. Dale, and J. F. Paulson, J. Chem. Phys. **67**, 793 (1977).
[20] T. L. Rose, D. H. Katayama, J. A. Welsh, and J. F. Paulson, J. Chem. Phys. **70**, 4542 (1979).
[21] D. C. McGilvery and J. D. Morrison, Int. J. Mass Spectrom. Ion Phys. **28**, 81 (1978).
[22] Given by $m_{min} = eV_0/\pi^2 q r_0^2 \nu^2$, where V_0 = peak-to-peak rf voltage, r_0 = field dimension = 8.29×10^{-3} m, ν = rf frequency, and $q \simeq 0.91$. Thus $m_{min} \simeq 14$ g/mol under our conditions.
[23] J. F. Paulson, F. Dale, and P. M. Hierl (unpublished data).
[24] T. L. Rose and J. F. Paulson (unpublished data).
[25] Rose *et al.* (see Ref. 24) obtained a larger σ_{NO} at the "3381 Å" peak than reported in our original paper (see Ref. 19) by raising the primary ion energies and improving the geometry of the interaction region to ensure collection of all photofragment ions.
[26] S. Abed, M. Broyer, M. Carre, M. L. Gaillard, and M. Larzilliere, Chem. Phys. **74**, 97 (1983).
[27] I. Nenner, P. M. Guyon, T. Baer, and T. R. Govers, J. Chem. Phys. **72**, 6587 (1980).
[28] R. Frey, B. Gotchev, W. B. Peatman, H. Pollak, and E. W. Schlag, Chem. Phys. Lett. **54**, 411 (1978).
[29] A. Carrington, D. R. J. Milverton, and P. J. Sarre, Mol. Phys. **32**, 297 (1976).
[30] T. F. Thomas, F. Dale, and J. F. Paulson, J. Chem. Phys. **79**, 4078 (1983).
[31] J. H. D. Eland and C. J. Danby, Int. J. Mass Spectrom. Ion Phys. **1**, 111 (1968).
[32] D. R. Lloyd and P. J. Roberts, Mol. Phys. **26**, 225 (1973).
[33] J. Erickson and C. Y. Ng, J. Chem. Phys. **75**, 1650 (1981).
[34] D. W. Turner, C. Baker, A. D. Baker, and C. R. Brundle, *Molecular Photoelectron Spectroscopy* (Wiley–Interscience, London, 1970), pp. 85, 126, 127.
[35] I. N. Levine, *Molecular Spectroscopy* (Wiley–Interscience, London, 1975), p. 254.
[36] S. Rothenberg and H. F. Schaefer III, J. Chem. Phys. **53**, 3014 (1970).
[37] I. H. Hillier and V. R. Saunders, Mol. Phys. **22**, 193 (1971).
[38] L. S. Cederbaum, W. Domcke, W. v. Niessen, and W. P. Kraemer, Mol. Phys. **34**, 381 (1977).
[39] H. Stein, M. Erben-Russ, and K. L. Kompa, J. Chem. Phys. **78**, 3774 (1983).
[40] S. P. Goss, R. G. McLoughlin, and J. D. Morrison, Int. J. Mass Spectrom. Ion Proc. **64**, 213 (1985).
[41] T. Shimanouchi, *Tables of Molecular Vibrational Frequencies*, NSRDS-Natl. Bur. Stand. No. 39 (U. S. GPO, Washington, D. C., 1972), Vol. I, p. 13.
[42] K. Kimura *et al.*, *Handbook of Hel Photoelectron Spectra of Small Molecules* (Halsted, New York, 1981), p. 40.
[43] C. P. Edwards, C. S. Maclean, and P. J. Sarre, Mol. Phys. **52**, 1453 (1984).
[44] C. S. Gudeman and R. J. Saykally, Annu. Rev. Phys. Chem. **35**, 387 (1984).
[45] According to the *ab initio* SCF/CI calculations of Hopper, the lowest energy quartet state of N_2O^+ ($1\,^4\pi$ in the linear configuration and $1\,^4A''$ in the bent) has a very long and shallow saddlepoint region but is not a bound state (see Refs. 47 and 48). Its potential energy surface does, however, have two local minima ("polarization wells")—one at large $R_{N\text{-}O}$ and one at large $R_{N\text{-}N}$ (see Refs. 46 and 47). Transitions from these wells to a higher quartet, e.g., $1\,^4\Sigma^+$—which correlates with formation of N_2^+ (see Ref. 46), could explain the minor photoproducts. Absorption by the metastable $1\,^2\delta$ state (see Ref. 46) is also a possibility.
[46] D. G. Hopper, J. Am. Chem. Soc. **100**, 1019 (1978).
[47] D. G. Hopper, J. Chem. Phys. **72**, 3679 (1980).
[48] D. G. Hopper, J. Chem. Phys. **76**, 1068 (1982).

Rate constants for quenching the $\tilde{A}\,^2A_2$ state of SO_2^+ by atmospheric gases

Timothy F. Thomas
Department of Chemistry, University of Missouri-Kansas City, Kansas City, Missouri 64110

Fred Dale and John F. Paulson
Air Force Geophysics Laboratory/LID, Hanscom AFB, Massachusetts 01731

(Received 11 August 1987; accepted 13 January 1988)

The effect of ion source pressure on the cross sections for photodissociation of SO_2^+ has been measured systematically at $\lambda_{irr} = 4735$ and 4795 Å. Using a Stern–Volmer treatment modified to account for the dependence of source residence time on pressure, rate constants have been measured for quenching the $\tilde{A}\,^2A_2$ $(v_1,v_2 = 3,3)$ and $\tilde{A}\,^2A_2(v_1,v_2 = 3,0)$ states of SO_2^+ by N_2O, SO_2, CO_2, and N_2. With SO_2 and N_2O as quenchers the rate constants range between 1.0 and 6.5 times the theoretical thermal capture rate constants ("Langevin limit"). The occurrence of several resonant and many near-resonant charge transfer processes is proposed to explain the unusually large rate constants.

I. INTRODUCTION

In the course of obtaining the ion photodissociation spectrum of SO_2^+, which we have recently reported in this Journal,[1] we have observed that the measured cross sections for photodissociation in the visible region were dependent upon the pressure of SO_2 used in the ion source. Since our previous work using the same ion source had shown no pressure effect on the photodissociation cross sections of N_2O^+,[2] this observation was unexpected. At source pressures in the 0.01 to 0.10 Torr range ($\sim 30\times$ the pressure used in gathering our previous SO_2^+ data) a significant effect on the photodissociation spectrum of Ar_2^+ had previously been observed in the same ion source, however.[3] This effect was interpreted in terms of collisional deactivation of vibrationally excited Ar_2^+ with a rate constant $\sim 12\%$ of Langevin. Thus, the pressure effect seen for SO_2^+ indicated some deactivation process occurring at a rate exceeding the theoretical upper limit for ion–molecular reactions. It therefore seemed important to make a systematic study of the processes involved and their precise rate constants.

II. EXPERIMENTAL METHOD

The ion photodissociation apparatus—a triple quadrupole system with coaxial irradiation of the ion beam by a flashlamp pumped dye laser—has been described in detail previously.[1] The first quadrupole transmitted only ions of a selected mass into the second quadrupole ("reactor quadrupole," with rf field only) where the only observable interaction with the laser beam occurred. The third quadrupole was adjusted to transmit either photoproduct ions or unreacted parent ions to the detector. Before beginning a systematic study of the pressure dependence of the photodissociation cross sections an MKS Baratron gauge equipped with a 1 Torr head was connected to one side of the ionization chamber via 1/4 in. o.d. (3/16 in. i.d.) tubing. Since sample gases flowed into the ionization chamber through a separate 1/4 in. o.d. tube connected at the opposite side of the chamber and the major escape path was through the 1/8 in. i.d. ion exit aperture (see the top half of Fig. 1), it was thought that the pressure measured in the Baratron head corresponded closely to that existing in the ionization region. There was no repeller in the ionization chamber.

Ions were produced by the impact of electrons accelerated through 50 V from a hot rhenium filament to the ionization chamber which they entered through a 1 mm hole. When the pressure in the ionization chamber was changed, the current through the filament was manually adjusted (in the opposite direction) to keep a constant ion beam current in the reactor quadrupole. Typically, the total emission from the filament was changed from 40 to $\leqslant 1.0\,\mu$A as the pressure in the ionization chamber was raised from 0.5 to 8.0 mTorr. This adjustment was intended to avoid changes in the ion beam profile and possible saturation effects on the ion-counting system which could have produced artificial pressure effects. No significant effect of changing *only* the filament emission on the photodissociation cross sections was observed.

In order to obtain quenching rate constants from the pressure dependence of the photodissociation cross sections it was necessary to determine the average residence time of the SO_2^+ ions in the ion source. For this purpose, about halfway through this study, a grid (82% transmitting Ni mesh) was installed between the filament and the ionization chamber, as shown in the top half of Fig. 1. This grid was normally biased slightly negative with respect to the filament until the arrival of a positive voltage pulse 0.4–0.5 μs wide from an EH 132 A-8 pulse generator, which caused a burst of electrons to enter the ionization chamber. A second pulse generator (Hewlett Packard 214 A), triggered by the first with a adjustable time delay, delivered a $+95$ V pulse, 0.4–0.5 μs wide, to the ion accelerating plate located next to the ion exit hole in the ionization chamber. The timing sequence for the pulses is shown in the lower half of Fig. 1. This second pulse produced a dip in the peak of ion counts seen on the time-of-flight spectrum of the ions produced by the initial burst of electrons, as shown in Fig. 2. The time delay (measured on a Tektronix 511 oscilloscope) between the two voltage pulses which centered the dip in the top of the TOF peak was taken to equal the average residence time in the ionization chamber (Υ_c) plus the flight time of the ions between the ion exit hole and the accelerating plate (Υ_f):

$$\Upsilon_m = \Upsilon_c + \Upsilon_f. \tag{1}$$

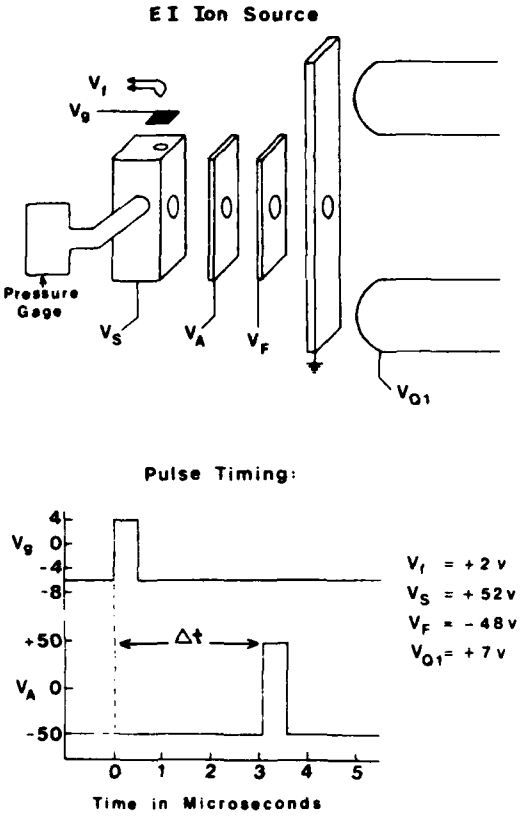

FIG. 1. Electron impact ion source (upper) and double-pulse timing sequence used to measure residence time in ion source (lower). V_f, V_g, V_S, V_A, and V_F designate the voltages applied to the filament, control grid, ionization chamber ("ion source"), ion accelerating plate, and focusing plate, respectively.

The flight time Υ_f was calculated from

$$\Upsilon_f = (2dm/eE)^{1/2}, \tag{2}$$

where d = the distance from the ion exit hole to the center of the accelerating plate = 2.86×10^{-3} m, E = the voltage gradient over that distance = 3.50×10^4 V m^{-1}, and m = the mass of the SO_2^+ ions. The calculated value was $\Upsilon_f = 0.33$ μs.

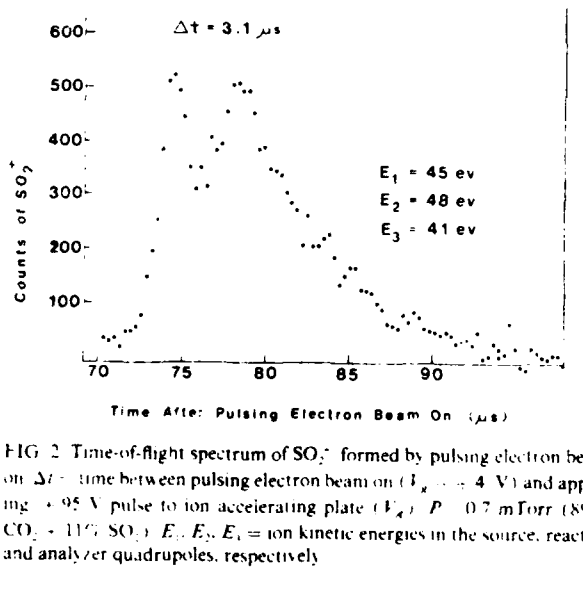

FIG. 2. Time-of-flight spectrum of SO_2^+ formed by pulsing electron beam on. Δt = time between pulsing electron beam on (V_g = +4 V) and applying +95 V pulse to ion accelerating plate (V_A). P = 0.7 mTorr (89% CO_2 + 11% SO_2). E_1, E_2, E_3 = ion kinetic energies in the source, reactor, and analyzer quadrupoles, respectively.

The values of Υ_m were found to increase linearly with the pressure in the ionization chamber. The best fit of the pressure dependence of the source residence times was given by

$$\Upsilon_s = 2.6(\pm 0.2) + 0.17(\pm 0.02)P, \tag{3}$$

where Υ_s is in μs and the pressure is in mTorr. The indicated error ranges are standard deviations from a least-squares fit to residence times determined at seven pressures ranging from 0.5$_6$ to 7.1 mTorr. Other equations tried, which were less accurate in fitting the observed pressure dependence, included: ln Υ_s vs P, Υ_s^{-1} vs P^{-1}, and Υ_s^{-1} vs $P^{-1/2}$. The latter two functions, predicted to describe the mobility of ions for low, and for moderately strong, ratios of electric field to gas density (E/N), respectively,[4] predict a stronger pressure dependence than actually observed. For the sake of comparison, the residence time of neutral molecules in the ion source was 1.2 ms when P = 3.2 mTorr.

Photodissociation cross sections measured after modifying the ion source for the double-pulse measurements of residence times showed a significantly smaller dependence on pressure than those measured before the modifications. This difference may be due to the effect of the control grid (biased 33 V positive with respect to the filament in the quenching experiments performed after the measurement of the source residence times) on the electric field inside the source. The two sets of quenching data were made consistent by multiplying the values of Υ_s calculated from Eq. (3) by the factor 2.05 before plotting the data from the earlier experiments in Figs. 4 and 5.

Gas mixtures were prepared on a stainless steel vacuum line equipped with three 1 ℓ storage bulbs and four Bourdon tube pressure gages (0–1000 Torr range, smallest scale division = 10 Torr). In the case of SO_2 + N_2O and SO_2 + CO_2 mixtures a measured amount of each gas was frozen from different storage bulbs into a single glass nipple, then flash vaporized into a third storage bulb which had previously been evacuated. In the case of SO_2 + N_2 known amounts of each gas were mixed by sudden expansion from their storage bulbs into the vacuum line, followed by a second rapid expansion into a third (evacuated) storage bulb. In this case the mixing was allowed to continue overnight. The compositions of the prepared mixtures, based on measured initial pressures, were: 80% N_2O + 20% SO_2; 89% CO_2 + 11% SO_2; and 89% N_2 + 11% SO_2. Mass spectral analyses run before and after using the mixtures confirmed these compositions within < 2% except for the case of N_2O + SO_2, which appeared to change from 80% to 87% N_2O during the two day period in which that mixture was used. The gases used to make the mixtures were all of stated purities > 99%; the SO_2, N_2O, and CO_2 were subjected to at least one freeze (to liquid N_2)–pump–thaw cycle to remove noncondensible impurities before use.

To confirm that the pressure in the ionization region was being measured accurately, and to obtain an estimate of the electric field present in the ionization region, a series of

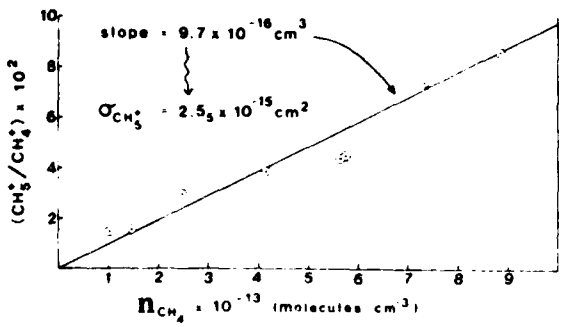

FIG. 3. Cross section measurement for $CH_4^+ + CH_4 \rightarrow CH_5^+ + CH_3$ in ion source of ion photodissociation spectrometer. $T \sim 50$ °C

surements was made of the extent of the reaction

$$CH_4^+ + CH_4 \rightarrow CH_5^+ + CH_3 \qquad (4)$$

which occurred when pure (Research Grade) CH_4 was introduced into the ion source. These experiments were carried out immediately following the quenching experiments using the same operating conditions for the triple quadupole mass spectrometer with the following exceptions: the ion energy in the second quadrupole (E_2) was changed from 3.9 to 16 eV; the rf voltage on the second quadrupole was reduced from 400 to 210 VAC; and both reactant (CH_4^+) ion currents were measured on a Faraday cup located at the end of the third quadrupole using a Cary 31 electrometer.

The observed dependence of the ratio of product ion current to reactant ion current upon the concentration of CH_4 in the ion source is shown in Fig. 3. The cross section for reaction (4) was calculated from Eq. (5),

$$\left(\frac{CH_5^+}{CH_4^+}\right) = \sigma l [CH_4], \qquad (5)$$

where l = the distance from the electron beam in the center of the ionization region to the ion exit hole = 0.38 cm. The result was $\sigma = 25.5$ Å^2. Comparison of this value with the literature data on the dependence of the cross section on average kinetic energy of the reactant ions[5,6] leads to the following value for the electric field strength present in our ion source: $E = 8.1$ V/cm.

The preceding result was used to calculate a theoretical ion source residence time, using an equation by Field, Franklin, and Lampe[7] (although in our case the electric field was due to penetration of fields from the ion accelerating plate and filament grid instead of established by a repeller plate), yielding $\Upsilon = 2.5$ μs. This time agrees with our measured source residence time at the $P = 0$ limit, within our indicated experimental error.

III. RESULTS

Figures 4 and 5 show the effect of pressure in the ionization region upon the reciprocal of the measured photodissociation cross section for several gas mixtures and two irradiation wavelengths. The method of plotting the data is a modification of the classical Stern–Volmer treatment, taking into account the variation in source residence time reported in Sec. II. Equations for analyzing these data were

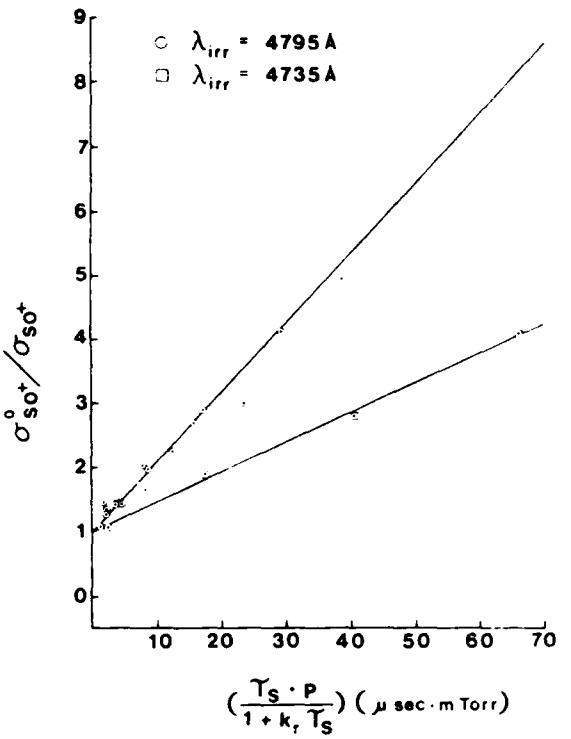

FIG. 4. Dependence of cross sections for $SO_2^+ + h\nu \rightarrow SO^+ + O$ on source pressure (P) and residence time (Υ_s). $\sigma^0_{SO^+}$ = limit of cross section when $p \rightarrow 0$; $k_r = 4.0 \times 10^4$ s^{-1}. For pure SO_2.

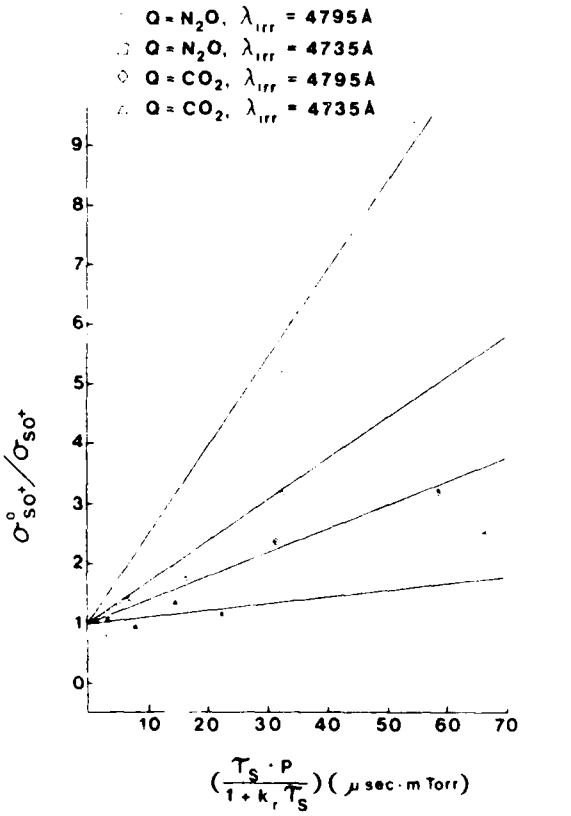

FIG. 5. Dependence of cross sections for $SO_2^+ + h\nu \rightarrow SO^+ + O$ on source pressure and residence time for mixed gases.

derived from the following scheme of fundamental processes occurring in the ion source:

Process	Rate	
$SO_2 + e^- \rightarrow SO_2^{+\dagger} + 2e^-$	$\alpha_1 i_{em}[SO_2]$,	(6)
$SO_2 + e^- \rightarrow SO_2^+ + 2e^-$	$\alpha_2 i_{em}[SO_2]$,	(7)
$Q + e^- \rightarrow Q^+ + 2e^-$	$\alpha_Q i_{em}[Q]$,	(8)
$SO_2^{+\dagger} + SO_2 \rightarrow SO_2^+ + SO_2^*$	$k_{SO_2}[SO_2^{+\dagger}][SO_2]$,	(9)
$SO_2^{+\dagger} + Q \rightarrow SO_2^+ + Q^*$	$k_e[SO_2^{+\dagger}][Q]$,	(10)
$SO_2^{+\dagger} + Q \rightarrow SO_2 + Q^+$	$k_{ce}[SO_2^{+\dagger}][Q]$,	(11)
$SO_2^{+\dagger} \rightarrow SO_2^+ + h\nu$	$k_r[SO_2^{+\dagger}]$,	(12)
$Q^+ + SO_2 \rightarrow SO_2^+ + Q$	$k_{rce}[Q^+][SO_2]$,	(13)
$SO^{+\dagger} \rightarrow (SO_2^{+\dagger})_{\text{ion beam}}$	$k_e[SO_2^{+\dagger}]$,	(14)
$SO_2^+ \rightarrow (SO_2^+)_{\text{ion beam}}$	$k_e[SO_2^+]$.	(15)

The first three processes shown are ionization by electron impact. The † designates an observable electronically excited state—in the case of the 4400–5200 Å portion of the photodissociation spectrum of SO_2^+ this refers to the metastable $\tilde{A}(^2A_2)$ state. The next three lines represent energy transfer processes, electronic (including charge transfer) and vibrational, which deplete the population of a particular energy level in $SO_2^{+\dagger}$ from which a transition originates for a given λ_{uv}. Q is the added gas whose quenching efficiency was measured. Step (12) allows for radiative decay from the metastable state. Steps (14) and (15) allow for escape from the ion source to the ion beam where the low density makes the rate of collisions insignificant.

Use of the steady state approximation for the concentration of the reactive intermediates in the above scheme yields the following expressions for the concentrations of $SO_2^{+\dagger}$ and SO_2^+ in the ion source:

$$[SO_2^{+\dagger}] = \frac{\alpha_1 i_{em}[SO_2]}{\beta + k_r + k_e} \tag{16}$$

and

$$[SO_2^+] = \frac{i_{em}}{k_e}\left\{\alpha_2[SO_2] + \alpha_Q[Q] - \frac{\beta\alpha_1[SO_2]}{\beta + k_r + k_e}\right\}, \tag{17}$$

where

$$\beta = k_{SO_2}[SO_2] + (k_{ce} + k_{rce})[Q]. \tag{18}$$

For a given gas mixture, introduced into the ion source at different total pressures but fixed composition, one can make the following substitution in Eqs. (16)–(18): $[SO_2] = X_{SO_2}P/RT$ and $[Q] = X_Q P/RT$, in which X_{SO_2} and X_Q are the mole fractions of SO_2 and the quenching gas, respectively. Then,

$$\beta = \frac{P}{RT}[X_{SO_2}k_{SO_2} + X_Q(k_{ce} + k_{rce})]. \tag{19}$$

The photodissociation cross sections previously reported for SO_2^+, as well as those measured in this work, were calculated using the total ion beam current in the laser–ion interaction region. For $\lambda_{uv} > 4187$ Å, however, only ions in the $\tilde{A}$ state (or higher) of SO_2^+ are capable of photodissociation. Thus, the observed cross sections are related to the true cross sections for processes originating in the $\tilde{A}$ state by

$$\sigma_{obs} = \left(\frac{[SO_2^{+\dagger}]\exp(-k_r t)}{[SO_2^{+\dagger}] + [SO_2^+]}\right)\cdot\sigma_{true}. \tag{20}$$

Equation (20) assumes the same relative population of the metastable ions in the ion beam as in the ion source except for a correction factor for radiative decay.[8] Substituting Eqs. (16)–(18) into Eq. (20) gives

$$\sigma_{obs} = \frac{k_e\alpha_1\sigma_{true}\exp(-k_r t)}{(k_r + k_e - \beta)\{\alpha_1 + \alpha_2 + (\alpha_Q[Q]/[SO_2])\}}. \tag{21}$$

In the limit of zero pressure (for fixed composition) $\beta = 0$, and

$$\sigma^0_{obs} = \frac{k_e\alpha_1\sigma_{true}\exp(-k_r t)}{(k_r + k_e)\{\alpha_1 + \alpha_2 + (\alpha_Q[Q]/[SO_2])\}}. \tag{22}$$

Dividing Eq. (22) by Eq. (21) yields

$$\frac{\sigma^0_{obs}}{\sigma_{obs}} = 1 + \frac{\beta}{k_r + k_e}. \tag{23}$$

Using Eq. (19) and $k_e = \Upsilon_e^{-1}$, where Υ_e is given by Eq. (3), converts Eq. (23) into the equation used to fit the pressure dependence of the photodissociation cross sections:

$$\frac{\sigma^0_{obs}}{\sigma_{obs}} = 1 + \frac{[X_{SO_2}k_{SO_2} + X_Q(k_{ce} + k_{rce})]}{RT}\cdot\left(\frac{\Upsilon_e}{1 + k_r\Upsilon_e}\right)P. \tag{24}$$

The experimental data obtained in the study are plotted in Figs. 4 ($X_Q = 0$) and 5 ($X_Q \neq 0$), using the previously determined value of $k_r = 4.0 \times 10^4\ s^{-1}$. The variables plotted are the same as in the classical Stern–Volmer treatment of fluorescence quenching, except that the pressure in the ion source is modified by a factor which accounts for the nonconstant residence time: $\Upsilon_e/(1 + k_r\Upsilon_e)$. Without this factor σ^0/σ vs P plots showed considerable curvature for pure SO_2 and for the $SO_2 + NO$ mixture. Ten points obtained using the $SO_2 + N_2$ mixture (five at each wavelength) were omitted from Fig. 5 for the sake of clarity. Values of k_{SO_2} were obtained from the slopes of the least-squares lines shown in Fig. 4, using $T = 323$ K in Eq. (24). These values of k_{SO_2} were then combined with the slopes of the lines shown in Fig. 5, and with the unplotted data for $SO_2 + N_2$, to obtain values for $k_{ce} + k_{rce}$ for $Q = N_2O$, CO, and N_2. The resulting rate constants, in molecular units, are shown in Table I. The indicated uncertainties are obtained from the standard deviations of the slopes of the lines in Figs. 4 and 5.

The rate constants were converted into the quenching cross sections, shown in the last column of Table I, using the relation

$$\sigma_Q = k/\bar{v}. \tag{25}$$

Here $\bar{v}$, the average velocity toward the exit hole of the ions in the ionization region, was estimated from l/Υ_e, where l was defined in Sec. II and Υ_e is the source residence time at the limit of zero pressure. The resulting value for SO_2^+ is $\bar{v} = 1.4 \times 10^5$ cm s^{-1}.

A short series of measurements of the pressure depen-

TABLE I. Quenching rate constants for SO_2^+ ($\tilde{A}\,^2A_2$).

Quencher	$10^9 \times k_{SO_2}$ ($cm^3\,s^{-1}$)	$10^9 \times (k_Q + k_{rr})$ ($cm^3\,s^{-1}$)	$\sigma_Q(Å^2)$
$\lambda_{irr} = 4735$ Å			
SO_2	1.55 ± 0.06		106 ± 4
N_2O		2.52 ± 0.29	173 ± 20
CO_2		0.22 ± 0.32	15 ± 22
N_2		−0.36 ± 0.20	−25 ± 14
$\lambda_{irr} = 4795$ Å			
SO_2	3.63 ± 0.12		249 ± 38
N_2O		5.38 ± 0.45	368 ± 31
CO_2		1.08 ± 0.20	74 ± 14
N_2		0.47 ± 0.20	32 ± 14

TABLE II. Selected ionization potentials and vibrational frequencies.[a]

Specie	Electronic state	IP(eV)	$\tilde{\nu}_1(cm^{-1})$	$\tilde{\nu}_2(cm^{-1})$	$\tilde{\nu}_3(cm^{-1})$
SO_2	$\tilde{X}\,^1A_1$	0	1167[a]	526[a]	1381[a]
SO_2^+	$\tilde{X}\,^2A_1$	12.311[b]	(1151)[c]	454[c]	(1362)[c]
SO_2^+	$\tilde{A}\,^2A_2$	13.030[c,d]	953[c]	499[c]	(1127)[c]
N_2O	$\tilde{X}\,^1\Sigma^+$	0	1285	589	2224
N_2O^+	$\tilde{X}\,^2\Pi_{3/2}$	12.886[e]	1126.5[f]	456.8[f]	1737.6[f]
N_2O^+	$\tilde{X}\,^2\Pi_{1/2}$	12.902[e,f]	1126.5[f]	456.8[f]	1737.6[f]
CO_2	$\tilde{X}\,^1\Sigma_g^+$	0	1333	667	2349
CO_2^+	$\tilde{X}\,^2\Pi_{3/2}$	13.776[g]	1266[g]	508[g]	1472[g]
N_2	$\tilde{X}\,^1\Sigma_g^+$	0	2359[h]		
N_2^+	$\tilde{X}\,^2\Sigma_g^+$	15.580[i]	2207[h]		

[a] All vibrational frequencies are from Ref. 26 unless otherwise noted; corrections for anharmonicity were applied in the case of SO_2 and SO_2^+ ($\tilde{A}$) only.
[b] Calculated from the fourth IP = 15.992 ± 0.003 eV for SO_2 (Ref. 27) and the tentatively assigned $\lambda_{00} = 3368 \pm 1$ Å for $\tilde{X}\,^2A_1 \rightarrow \tilde{C}\,^2B_1$ in SO_2^+ (Ref. 1). Previously reported values for the first IP of SO_2 are 12.30$_4$ ± 0.01 (Ref. 12) and 12.348 ± .002 eV (Ref. 28).
[c] From Ref. 1. ν_2 and ν_3 in the $\tilde{X}$ state were taken to be the same as for SO_2 (Ref. 26) and ν_1 in the $\tilde{A}$ state was estimated assuming $\tilde{\nu}_1/\tilde{\nu}_1 = 1.183$.
[d] Calculated from the fourth IP = 15.992 ± 0.003 eV for SO_2 (Ref. 27) and $\lambda_{00} = 4187 \pm 1$ Å for $\tilde{A}\,^2A_2 \rightarrow \tilde{C}\,^2B_1$ in SO_2^+ (Ref. 1).
[e] ± 0.002 eV, from Ref. 29. Other reported values are 12.889 (Ref. 30) and 12.893 ± .005 eV (Ref. 31).
[f] The $\tilde{\nu}_1$ and the $^2\Pi_{3/2}$–$^2\Pi_{1/2}$ splitting are from Ref. 25.
[g] From Ref. 32.
[h] From Ref. 33.
[i] From Ref. 34.
[j] From Ref. 35.

dence of the photodissociation cross sections was made in the UV spectrum of SO_2^+, using pure SO_2 and $\lambda_{irr} = 3192$ Å. The cross sections were found to *increase* with increasing source pressure (in contrast to the data in the visible region) up to $P \sim 3$ mTorr, where a maximum was reached. Above 3 mTorr the cross sections began to decrease slowly with pressure; at higher pressures the value of $d(\sigma^0/\sigma)/d(P \cdot Y_+)$ approximated that found for the 89% N_2 + 11% SO_2 mixtures at $\lambda_{irr} = 4795$ Å. Since the major transition occurring at 3192 Å is thought to be $\tilde{X}\,^2A_1 \rightarrow \tilde{C}\,^2B_1$, the low pressure results seem to confirm step (9), which augments the population of the $\tilde{X}$ state of SO_2^+, in the proposed quenching mechanism. The weaker pressure effect above 3 mTorr is consistent with a contribution at 3192 Å from an $\tilde{X} \rightarrow \tilde{C}$ transition originating from an excited vibrational level (we estimate that the $1_1^4 2_4^4$, $1_0^3 2_3^3$, and $1_0^2 2_2^4$ bands, e.g., would lie near 3192 Å). Another possible contributor would be a second electronic transition, such as $\tilde{A}\,^2A_1 \rightarrow \tilde{D}\,^2B_1$ (for which we predict an origin of $\lambda_{00} = 3792$ Å).

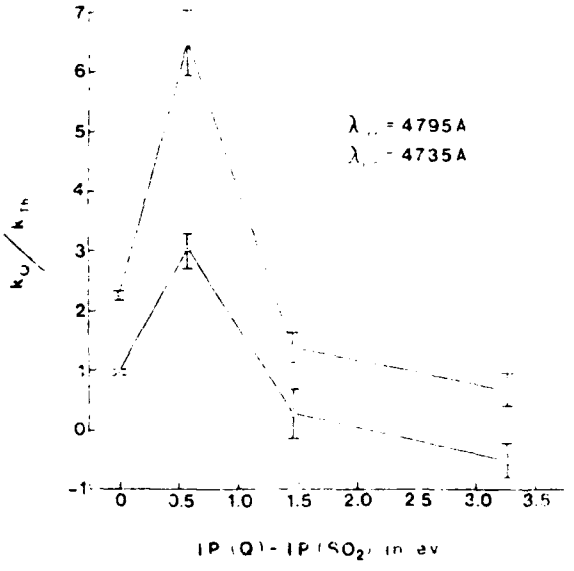

FIG. 6. Quenching rate constants as a function of difference in first ionization potentials of quenchers and SO_2. $k_Q = k_{rr}$ for pure SO_2. k_Q for Q = N_2O, CO_2, and N_2.

IV. DISCUSSION

The ratios of the experimentally determined quenching rate constants to theoretical rate constants are plotted vs the differences between the first ionization potentials of the quenchers and SO_2 in Fig. 6. The "theoretical" rate constants are thermal capture rate constants for collisions of SO_2^+ and the quencher, calculated using the parametrization of Su and Chesnavich,[10] which was estimated by those authors to be accurate to $< 3\%$. We used the following polarizabilities and dipole moments in the calculations: $\alpha = 4.28(SO_2)$, $3.03(N_2O)$, $2.91(CO_2)$, and $1.74(N_2)$ Å^3; $\mu = 1.63(SO_2)$ and $0.16(N_2O)$ D.[11] The strong dependence of k_Q/k_{th} on the ionization potential of the quencher indicates that electronic energy transfer is the major pathway for quenching, at least for Q = SO_2 and N_2O. The "peak" observed in Fig. 6 matches well with the location of the $\tilde{A}$ state of SO_2^+, which lies 0.719$_4$ eV above the $\tilde{X}$ state (see Table II). This observation provides further confirmation that it is the $\tilde{A}$ state of SO_2^+ which is being quenched at $\lambda_{irr} = 4735$ and 4795 Å.

A brief review of recent literature on the quenching of excited states of ions by small neutral molecules shows the following trends:

(a) Quenching rate constants usually increase with increasing vibrational quantum number in the donor.[13–17]

(b) Ions in electronically excited states react more rapidly than the corresponding ions in ground electronic states.[18–20]

(c) An applied electric field (increasing ion velocity), has

only a small effect on the rate of some exothermic charge transfer reactions of O_2^+ [17,19,21] but a stronger effect on charge transfer from CO_2^+, N_2O^+, and SO_2^+.[22] It is generally assumed, however, that the rate constant never exceeds k_{Th}.

It has also commonly been accepted that a small ΔE and large Franck–Condon factors are necessary for the quenching process to be fast.[14,15,37,38] In the present study the ions being quenched are highly vibrationally excited ($v_1 = 3$ for both wavelengths used, plus $v_2 = 3$ when $\lambda_{irr} = 4795$ Å) as well as electronically excited so that large quenching rate constants would be expected if ΔE is small and the Franck–Condon factors are favorable. Figure 6 also shows that all k_Q's increase when v_2 is increased from 0 ($\lambda_{irr} = 4735$ Å) to 3 ($\lambda_{irr} = 4795$ Å).

In the case where $Q = N_2O$ the following processes are calculated, using the data shown in Table II, to provide essentially resonant pathways for quenching by charge exchange[23]:

$$SO_2^+(\tilde{A}\,^2A_2,330) + N_2O \rightarrow SO_2(340) + N_2O^+(\tilde{X}\,^2\Pi_{3/2},000), \quad \Delta E = 108\ cm^{-1}, \tag{26}$$

$$SO_2^+(\tilde{A}\,^2A_2,300) + N_2O \rightarrow SO_2(310) + N_2O^+(\tilde{X}\,^2\Pi_{3/2},000), \quad \Delta E = -6\ cm^{-1}. \tag{27}$$

Not only is ΔE nearly zero, within the combined uncertainty ($\pm 50\,cm^{-1}$) of the two ionization potentials used to calculate the quantity, but the Franck–Condon factors should be large also because $\Delta v_1 = 0$ and $\Delta v_2 = 1$ to 8 for the strongest peaks in the first band of the photoelectron spectrum of SO_2[12] and the largest Franck–Condon factor for ionization of N_2O corresponds to the $\tilde{X}\,^1A_1 \rightarrow \tilde{X}\,^2\Pi_{3/2},000$ transition.[24]

In addition to reactions (26) and (27), 43 exothermic charge transfer processes are predicted to be possible from the $v_1v_2v_3 = 330$ vibrational level and 34 processes from the 300 level of the $\tilde{A}$ state of SO_2^+, to yield either the $\tilde{X}\,^2\Pi_{3/2}$ or $\tilde{X}\,^2\Pi_{1/2}$ states of N_2O^+, subject to the restriction that $v_1 \leq 3$ and $v_2 \leq 5$ in the neutral SO_2 product. Still more exothermic processes may be written yielding N_2O^+ with $v_2 = 1$ or 2, which vibrational levels are split by the Renner effect into ten states lying within 0.139 eV (1122 cm^{-1}) of $\tilde{X}\,^2\Pi_{1/2},000$.[25] One example of such a process is

$$SO_2^+(\tilde{A}\,^2A_2,330) + N_2O \rightarrow SO_2(330) + N_2O^+(\tilde{X}\,^{\infty}\Sigma_{1/2}^{(+)},010), \quad \Delta E = +27\ cm^{-1}, \tag{28}$$

where the notation used for the spin-vibronic level of N_2O^+ is taken from Callomon and Creutzberg.[25] The rate constants listed under the heading "$k_v + k_{ce}$" for $Q = N_2O$ in Table I are the sums of the rate constants for all processes which depopulate the previously indicated excited states. Based on the results obtained with $Q = CO_2$ and N_2 (see below), however, we conclude that $k_{ce} \gg k_v$ when $Q = N_2O$ or SO_2.

In the case where $Q = SO_2$, step (9) in the reaction scheme proposed above includes two distinct processes. The first process is collision-induced internal conversion of SO_2^+ from the $\tilde{A}\,^2A_2$ state to the $\tilde{X}\,^2A_1$ state with the decrease in electronic energy of the ion equaling the increase in its vibrational energy. Examples of this process for the two vibronic states of SO_2^+ whose quenching rates were measured in our study are

$$SO_2^+(\tilde{A}\,^2A_2,330) + SO_2 \rightarrow SO_2^+(\tilde{X}\,^2A_1,590) + SO_2, \quad \Delta E = -111\ cm^{-1}, \tag{29}$$

$$SO_2^+(\tilde{A}\,^2A_2,300) + SO_2 \rightarrow SO_2^+(\tilde{X}\,^2A_1,560) + SO_2, \quad \Delta E = -90\ cm^{-1}. \tag{30}$$

Since $\Delta v_1 = +2$ for the ion, the Franck–Condon factors may not be as large as for reactions (26) and (27). Also, the calculated ΔE's may not be very accurate since no anharmonicity constants were available to use for predicting vibrational energies in the $\tilde{X}$ state of SO_2^+.

The second quenching process when $Q = SO_2$ is charge transfer. Example reactions which are nearest to resonance (subject to the restrictions $\Delta v_1 = \Delta v_2 = 0$ in the donor and $v_1 \leq 5$, $v_2 \leq 10$ in the product ion) are

$$SO_2^+(\tilde{A}\,^2A_2,330) + SO_2 \rightarrow SO_2(330) + SO_2^+(\tilde{X}\,^2A_1,260), \quad \Delta E = +21\ cm^{-1}, \tag{31}$$

$$SO_2^+(\tilde{A}\,^2A_2,300) + SO_2 \rightarrow SO_2(300) + SO_2^+(\tilde{X}\,^2A_1,410), \quad \Delta E = -80\ cm^{-1}. \tag{32}$$

Subject to the same restrictions, another exothermic 31 and 32 state-to-state reactions may be written for $v_1v_2v_3 = 330$ and 300 levels of SO_2^+ ($\tilde{A}$), respectively.

In the case where $Q = CO_2$ charge transfer from the $\tilde{A}$ state of SO_2^+ is endothermic by $6013 \pm 50\ cm^{-1}$. Thus, $k_{ce} \ll k_v$ would be expected. This expectation is supported by the fact that k_Q (4795 Å) $\sim 5 \cdot k_Q$ (4735 Å) reflecting the greater ease of transferring a quantum from the low energy bending mode ($\tilde{\nu}_2$) via

$$SO_2^+(\tilde{A}\,^2A_2,330) + CO_2 \rightarrow SO_2^+(\tilde{A}\,^2A_2,320) + CO_2(010), \quad \Delta E = +251\ cm^{-1} \tag{33}$$

than from the higher energy symmetric stretching mode via

$$SO_2^+(\tilde{A}\,^2A_2,300) + CO_2 \rightarrow SO_2^+(\tilde{A}\,^2A_2,200) + CO_2(100), \quad \Delta E = +421\ cm^{-1}. \tag{34}$$

It is also possible that quenching by CO_2 could occur via collision-induced internal conversion, analogous to reactions (29) and (30). It is not clear, however, why the rate constant for internal conversion should decrease by factors of 3.4 (at 4795 Å) and 7 (at 4735 Å) when the quencher is changed from SO_2 to CO_2. *A simpler interpretation of all our data is that the faster quenching by SO_2 and N_2O proceeds predominantly by charge transfer and that the results obtained for CO_2 measure the combined rate of V–V energy transfer and collision-induced internal conversion.*

The still smaller quenching rate constants obtained for $Q = N_2$ reflect the fact that the transfer of a single vibrational quantum would be endothermic by an amount much greater than $3/2\,RT$ (340 cm^{-1}):

$$SO_2^+(\tilde{A}\,^2A_2,330) + N_2 \rightarrow SO_2^+(\tilde{A}\,^2A_2,230) + N_2(1), \quad \Delta E = +1465\ cm^{-1}. \tag{35}$$

The negative value of the rate constant for quenching the $v_1v_2v_3 = 300$ level of the $\tilde{A}$ state of SO_2^+ is probably real, resulting from the rate of populating it by collision from

TABLE III. Selected charge transfer rate constants exceeding Langevin.

No.	Reaction	T(K)	$KE_{c.m.}$ (eV)	k_{ce}/k_{Th}	Method	Reference
(1)	$Ar_2^+ + CS_2 \rightarrow 2Ar + CS_2^+$	300	0.55	1.26 ± 0.06	SIFT-DRIFT	36
(2)	$D_2^+ (v=1) + N_2 \rightarrow D_2 + N_2^+$	~400	1.0	1.48 ± 0.37	PIRFG[b]	37
(3)	$H_2^+ (v=1) + N_2 \rightarrow H_2 + N_2^+$	~400	1.0	1.60 ± 0.40	PIRFG[b]	37
(4)	$N_2^+ (\tilde{B}\,^2\Sigma_u^+, v=1) + N_2 \rightarrow N_2 + N_2^+$	300	···	1.83 ± 0.28	FDQ[c]	16
(5)	$NO^+ (\tilde{a}\,^1\Sigma^+, v=2) + Ar \rightarrow NO + Ar^+$	~300	1.4	2.06	TESICO[d]	38
(6)	$H_2^+ (v=0) + CO \rightarrow H_2 + CO^+$	~400	1.0	2.17 ± 0.54	PIRFG	37
(7)	$SO_2^+ (\tilde{A}\,^2A_2, v_1v_2=33) + SO_2 \rightarrow SO_2 + SO_2^+$	323	0.7,[e]	$2.2_5 \pm 0.07$	IPDS[e]	This work
(8)	$SO_2^+ (\tilde{A}\,^2A_2, v_1v_2=30) + N_2O \rightarrow SO_2 + N_2O^+$	323	0.6,[e]	$3.0_4 \pm 0.35$	IPDS	This work
(9)	$D_2^+ (v=0) + CO \rightarrow D_2 + CO^+$	~400	1.0	$3.2_2 \pm 0.80$	PIRFG	37
(10)	$SO_2^+ (\tilde{A}\,^2A_2, v_1v_2=33) + N_2O \rightarrow SO_2 + N_2O^+$	323	0.6,[e]	$6.4_4 \pm 0.54$	IPDS	This work

[a] Selected ion flow tube with electric drift field added. Ions produced by electron impact.
[b] Ions produced by photoionization in radio frequency ion guide, then beamed through a scattering cell filled with neutral reactant.
[c] From measurement of fluorescence decay rate as function of pressure of quenching gas.
[d] Threshold electron–secondary ion coincidence technique, with mass analysis of products from reaction of ion beam with neutral gas. k_{ce} is derived from a cross section calculated using the theoretical method of Rapp and Francis (Ref. 39).
[e] Ion photodissociation spectroscopy. The $KE_{c.m.}$ shown is an average value; the full range of values for ions formed in our ion source is $KE_{c.m.} = 0 \rightarrow 1.54$ eV when $Q = SO_2$ and $0 \rightarrow 1.26$ eV when $Q = N_2O$

levels with $v_2 > 0$ being faster than the rate of depopulating it by removing a quantum from $v_1 = 3$. This effect of collision on the cascading from higher to lower energy levels does, of course, complicate the interpretation of all our data, but we believe it to be of minor importance in the cases of the larger rate constants measured.

As mentioned above it is often assumed that the thermal capture rate constants calculated by equations such as Su and Chesnavich's[10] provide an upper limit to experimentally determined rate constants for ion–molecule reactions. The results which we show in Table I and Fig. 6, however, exceed that upper limit by up to a factor of 6.5. It must be acknowledged that our k_Q's are *not* strictly thermal rate constants, since our SO_2^+ ions acquire a kinetic energy of ≤ 3.08 eV while being accelerated out of our ion source by the field penetrating from the ion accelerating plate. We feel, however, that the effect of ion kinetic energy is unlikely to be large enough to entirely account for the large k_Q/k_{Th} ratios we observed. Of greater significance is the combined effect of vibrational and electronic excitation and the existence of many resonant or near-resonant channels by which charge transfer can occur.

To put our results in perspective three of our rate constants are compared in Table III with seven other recently determined rate constants which exceed k_{Th} by at least 25%. In all cases except the first one specific vibronic states were monitored. Most measurements of the rate of ion–molecule reactions yield rate constants averaged over many vibrational states, and possibly even over several electronic states, thus obscuring any very fast resonant processes. The very strong enhancement of rate constants for processes having $\Delta E < RT$ (~ 210 cm^{-1} in our case) has been shown by Kato *et al.*, who calculate that 50% of reaction (5) in Table III proceeds via the state specific process:

$$NO^+ (\tilde{a}\,^1\Sigma^+, v=2) + Ar \rightarrow NO(\tilde{X}\,^1\Pi_{1/2}, v=1) + Ar^+ (^2P_{3/2}), \quad \Delta E = -137 \text{ cm}^{-1} \qquad (36)$$

although a total of 28 channels were energetically attainable at the collision energy used. The model used in the calculation of Kato *et al.* applies to charge transfer occuring via a simple electron jump mechanism at large interaction distances. This model would appear to be appropriate to describe the major part of the quenching of SO_2^+ ($\tilde{A}\,^2A_2$) by N_2O and by SO_2 and, as shown above, a number of channels exist in these cases which have even smaller ΔE's than does Eq. (36).

Based on our results and the above considerations, we suggest that many more reactions having $k_{ce} \gg k_{Th}$ can be discovered using recently developed techniques for studying state-to-state reactions between ions and molecules in which $\Delta E < RT$.

ACKNOWLEDGMENTS

The experimental work reported here was carried out at the Air Force Geophysics Laboratory while T.F.T. was an AFOSR-URRP Visiting Professor there. Support by Air Force Systems Command Contract No. F19628-84-K-0038 during the subsequent period of data analysis and manuscript preparation is gratefully acknowledged.

[1] T. F. Thomas, F. Dale, and J. F. Paulson, J. Chem. Phys. **84**, 1215 (1986).
[2] T. F. Thomas, F. Dale, and J. F. Paulson, J. Chem. Phys. **67**, 793 (1977).
[3] T. L. Rose, D. H. Katayama, J. A. Welsh, and J. F. Paulson, J. Chem. Phys. **70**, 4542 (1979).
[4] E. W. McDaniel and E. A. Mason, *The Mobility and Diffusion of Ions in Gases* (Wiley, New York, 1973), pp. 121–2.
[5] L. Friedman, in *Ion–Molecule Reactions in the Gas Phase*, Advances in Chem. Ser. No. 58 (American Chemical Society, Washington, D.C., 1966), p. 101.
[6] A. Giardini-Guidoni and L. Friedman, J. Chem. Phys. **45**, 937 (1966).
[7] F. H. Field, J. L. Franklin, and F. W. Lampe, J. Am. Chem. Soc. **79**, 2419 (1957).
[8] Under typical operating conditions t, the average flight time from the source to the region where photodissociation occurred (the center of the reactor quadrupole) was $\sim 48\ \mu$s. Using the previously determined value of $k_r = 4.0 \times 10^3$ s^{-1} (Ref. 9) gives $\exp(-k_r t) = 0.15$; thus, the previously published cross sections should be multiplied by 6.8 in the visible region to compensate for radiative decay from the metastable state formed in the ion source.

[9]T. F. Thomas, F. Dale, and J. F. Paulson, J. Chem. Phys. 79, 4078 (1983).
[10]T. Su and W. J. Chesnavich, J. Chem. Phys. 76, 5183 (1982).
[11]C. G. Gray and K. E. Gubbins, *Theory of Molecular Fluids. Vol. I. Fundamentals* (Oxford University, Oxford, 1984), Appendix D.
[12]J. H. D. Eland and C. J. Danby, J. Mass Spectrom. Ion Phys. 1, 111 (1968).
[13]V. E. Bondybey and T. A. Miller, J. Chem. Phys. 69, 3597 (1978).
[14]D. H. Katayama, T. A. Miller, and V. E. Bondybey, J. Chem. Phys. 72, 5469 (1980).
[15]D. H. Katayama and J. A. Welsh, J. Chem. Phys. 79, 3627 (1983); Chem. Phys. Lett. 106, 74 (1984).
[16]J. Jolly and A. Plain, Chem. Phys. Lett. 100, 425 (1983).
[17]H. Bohringer, M. Durup-Ferguson, D. W. Fahey, F. C. Fehsenfeld, and E. E. Ferguson, J. Chem. Phys. 79, 4201 (1983).
[18]J. Glosik, A. B. Rakshit, N. D. Twiddy, N. G. Adams, and D. Smith, J. Phys. B 11, 3365 (1978).
[19]W. Lindinger, D. L. Albritton, M. McFarland, F. C. Fehsenfeld, and A. L. Schmeltekopf, J. Chem. Phys. 62, 4101 (1975).
[20]T. Ibuki and N. Sugita, J. Chem. Phys. 79, 5392 (1983); 80, 4625 (1984).
[21]I. Dotan, Chem. Phys. Lett. 75, 509 (1980).
[22]M. Durup-Ferguson, H. Bohringer, D. W. Fahey, and E. E. Ferguson, J. Chem. Phys. 79, 265 (1983).
[23]The "330" in reaction (26) means $v_1 = 3$, $v_2 = 3$, $v_3 = 0$ quanta in the three vibrational modes of SO_2^+, and so forth through subsequent reactions.
[24]H. M. Rosenstock, Int. J. Mass Spectrom. Ion Phys. 7, 33 (1971).
[25]J. H. Callomon and F. Creutzberg, Phil. Trans. R. Soc. London Ser. A 277, 157 (1974).
[26]T. Shimanouchi, *Table of Vibrational Frequencies*, Natl. Stand. Ref. Data Ser., Natl. Bur. Stand. No. 39 (U.S. GPO, Washington, D.C., 1972), Vol. 1.
[27]D. R. Lloyd and P. J. Roberts, Mol. Phys. 26, 225 (1973).
[28]J. Ericson and C. Y. Ng, J. Chem. Phys. 75, 1650 (1981).
[29]J. Berkowitz and J. H. D. Eland, J. Chem. Phys. 67, 2740 (1977).
[30]Y. Tanaka, A. S. Jursa, and F. J. LeBlanc, J. Chem. Phys. 32, 1205 (1960).
[31]C. R. Brundle and D. W. Turner, Int. J. Mass Spectrom. Ion Phys. 2, 195 (1969).
[32]A. W. Potts and G. H. Fattahallah, J. Phys. B 13, 2454 (1980).
[33]K. P. Huber and G. Herzberg, *Molecular Spectra and Structure. IV. Constants of Diatomic Molecules* (Van Nostrand Reinhold, New York, 1979).
[34]M. Ogawa and Y. Tanaka, Can. J. Phys. 40, 1593 (1962).
[35]R. D. Shelton, A. H. Nielson, and W. H. Fletcher, J. Chem. Phys. 21, 2178 (1953).
[36]R. J. Shul, R. Passarella, X. I. Yang, R. G. Keesee, and A. W. Castleman, Jr., J. Chem. Phys. 87, 1630 (1987).
[37]S. L. Anderson, T. Turner, B. H. Mahan, and Y. T. Lee, J. Chem. Phys. 77, 1842 (1982).
[38]T. Kato, K. Tanaka, and I. Koyano, J. Chem. Phys. 79, 5969 (1983).
[39]D. Rapp and W. E. Francis, J. Chem. Phys. 37, 2631 (1962).